

The Static Heavy Quark-Antiquark Potential within String Theory in Arbitrary Stationary Backgrounds

Nikita Tsegelnik*

Joint Institute for Nuclear Research, Dubna, 141980 Russia

(Dated: 15 Jun 2026)

We analyze a static open string in a general stationary spacetime, which can represent a heavy quark-antiquark pair within the holographic framework or effective theory. We establish that for a simple U-shaped string with only radial dependence on the space string coordinate, $x'_r(\sigma) \neq 0$, the string is generally not symmetric about its turning point, and the symmetry restores only for backgrounds with $h_{pr} = G_{00}G_{pr} - G_{0p}G_{0r} = 0$. Consequently, such asymmetric strings directly probe a possibility of the parity violation in the quark-antiquark interaction. Nevertheless, we identify a wide family of metrics for which the symmetry is preserved, enabling a direct isolation of the linear-in-distance term in the static interquark potential for simple symmetric string configurations, even in non-diagonal backgrounds. Applying the holographic framework, we further study the Rindler-AdS spacetime dual to an accelerated $\mathcal{N} = 4$ super Yang-Mills plasma. We show that the distance between quarks decreases, the static potential between them increases, and the deconfinement phase transition temperature, $T_{\text{dec}} = (\pi/3)T_H = a_c/6$, increases with an acceleration. However, we observe that an acceleration-scaled potential as a function of the acceleration-scaled distance does not depend on the certain value of the acceleration. This result, reflecting the scale invariance and self-similarity of the holographic setup, can be also obtained in the dimensionless metric after scaling of the coordinates onto the acceleration, $\tilde{x}_i = a_c x_i$, for which one obtains an universal value of the phase transition temperature, $\tilde{T}_{\text{dec}} = (\pi/3)\tilde{T}_H = 1/6$.

I. INTRODUCTION

Since the beginning of the 21st century, there has been active research into Quantum Field Theory (QFT) in the presence of external fields or under extreme conditions. Such conditions — extreme temperatures, densities, rotation, acceleration, background electromagnetic fields or condensates — can fundamentally alter the theory dynamics. They may affect phase transitions, stabilize or destabilize various structures, or give rise to entirely new novel phenomena. These studies are crucial not only from a theoretical standpoint, but also for interpreting modern high-energy experiments, where such extreme states are routinely created.

A prominent example is the physics of heavy-ion collisions (HIC), where generated electromagnetic fields are among the strongest in the known universe. It has been predicted that magnetic fields reaching up to 10^{18} Gauss may arise in non-central collisions [1–9]. Such fields can significantly modify the Quantum Chromodynamics (QCD) behavior, catalyzing the deconfinement and chiral transitions via the inverse magnetic catalysis [10–16], inducing anomalous transport within the Chiral magnetic effect [17–20], and generating the spin polarization [21–26]. Recently, the possibility of relatively long-lived, strong electric fields has also been explored [27], offering a direct probe of non-perturbative vacuum decay and pair production via the Schwinger mechanism [28–30].

Another rapidly growing direction involves non-inertial effects in QFT, which have gained considerable community interest following the observation of global spin polarization in HIC [31–34]. Contrary to early naive expectations of zero averaged polarization [35] and first controversial experimental evidences [36, 37], these observations have spurred a comprehensive re-examination of the spin theory [21, 38–47], establishing the thermal vorticity [39, 48, 49], consisting of rotation, acceleration, and temperature gradients, as the dominant source of the observed polarization signal in HIC.

Large angular momentum of the initial system, huge pressure and temperature gradients lead to the generation of the vorticity [50–54]. Detailed modelling of the velocity and vorticity fields [39, 48, 49, 52, 54–61] indicate that the medium created in heavy-ion collisions exhibits extreme local rotation $\omega \sim 10^{21} - 10^{23} \text{ sec}^{-1}$ and undergoes rapid collective expansion, whose early-time Hubble parameter exceeds the cosmological value by roughly 40 orders of magnitude. Notable, these predictions of the extreme values of the vorticity lead to the statement that QGP is a fastest-rotating fluid in nature [32, 62]. Recently, it was also shown that acceleration of the nuclear medium may reach extremely high values $a \sim 1 \text{ GeV}$ [63].

* tsegelnik@theor.jinr.ru

All of these extreme kinematic conditions motivate wide theoretical studies of QFT in rotating [64–87] and accelerated [88–105] medium. It is also essential to note the combined researches including rotation and electromagnetic fields [106–111]. Notably, recent lattice QCD calculations reveal striking results: the deconfinement (or chiral restoration) critical temperature exhibits opposite responses to rotation in the gluonic and fermionic sectors [112–117], negative moment of inertia and rotational instability of QGP [118–124].

These extreme conditions — strong external fields, rotation, acceleration, and high temperature/density — often correspond to strongly coupled regimes where traditional perturbative QCD methods fail. This strongly motivates the use of non-traditional methods, such as gauge/gravity duality, particularly the AdS/CFT correspondence [125], as a powerful non-perturbative tool [126–128]. By mapping a gauge theory in $D - 1$ dimensions to a classical gravitational theory in D -dimensional anti-de Sitter (AdS) space, holography provides geometric insight into a strongly coupled regime of the gauge theory.

In particular, the holography framework is successfully used in application to the calculations of the potential energy of the static quark-antiquark pair [129–139], studies of the confinement and deconfinement phases [140–151], evaluations of the energy losses [152–157], and other problems [158–180]. There are also a lot of researches in presence of the electromagnetic fields (finite chemical potential and baryon density) [181–191], rotation [181, 192–213], both of them [214–222], and uniform acceleration alone or in combinations with aforementioned fields [223–246].

A powerful probe for understanding how these extreme conditions affect strongly coupled nuclear matter is the static heavy quark-antiquark potential. Within the string theory, applicable both in holographic approach and in 4-dimensional string-based effective models of QCD, this potential is computed from the world sheet action of a (classical) string, the endpoints of which represent the (infinitely) heavy static quark and antiquark.

Specifically, in a gauge-theory context, the expectation value of a rectangular temporal Wilson loop $W(C)$, defined over a time interval $T \rightarrow \infty$ and a spatial separation L , is governed by the dynamics of the underlying flux tube. In the limit where the flux tube is well-described by a thin, classical string, the dominant contribution comes from the minimal-area world sheet spanning the contour C . This yields the relation

$$\langle W(C) \rangle \sim e^{-TV(L)} = e^{-S_{\text{NG}}[\Sigma]}, \quad (1)$$

where $S_{\text{NG}}[\Sigma]$ is the (renormalized) Nambu–Goto action evaluated on the corresponding surface Σ . The static quark-antiquark potential is therefore extracted as

$$V(L) = \lim_{T \rightarrow \infty} \frac{S_{\text{NG}}[\Sigma]}{T}. \quad (2)$$

The key advantage of this approach is its generality: the background metric in the string action can encode not only the geometry of a holographic bulk but also the effective spacetime felt by a flux tube in a thermal, rotating, electromagnetically polarized and other medium. In this paper, we will focus on arbitrary stationary spacetimes for several compelling reasons. First, a vast and physically relevant class of backgrounds is stationary: pure AdS, AdS black branes and black holes, Rindler-AdS, geometries with instantons or scalar condensates, and many solutions describing equilibrium states with rotation or external fields. Second, since we are interested in the static quark-antiquark potential ($T \rightarrow \infty$), the relevant string world-sheet probes a time-independent configuration. Third, while stationary metrics retain a high degree of physical generality, their time-independence substantially simplifies the equations of motion (EoM), allowing us to derive closed analytic expressions even in the presence of off-diagonal metric components. By working with a general stationary metric, we therefore obtain universal, tractable formulas for $V(L)$ that are applicable across a wide spectrum of holographic and effective string-based models of strongly coupled matter.

The paper is organized in the following way. In Sec. II, starting from a general stationary spacetime, we calculate the static interquark potential and analyze several important simplifications of the background metric. We find that the EoM generally does not preserve the symmetry with respect to the string turning point, hence, such configurations may probe parity violation effects in QCD. Restricting ourself by considering only simple symmetric U-shaped string, we show that even for a non-diagonal setup one can directly isolate the linear-in-distance term. In Sec. III we apply our general formulas to analysis of the static potential in the Rindler-AdS background in the holographic approach to study the accelerated $\mathcal{N} = 4$ super Yang-Mills plasma, the details of the analytical calculations of which we give in the App. A. In Sec. IV we conclude and discuss obtained results and prospects.

II. THE STATIC QUARK-ANTIQUARK POTENTIAL IN ARBITRARY STATIONARY BACKGROUND

The background and string configuration

We consider a D -dimensional stationary spacetime ($D \geq 3$) with the non-diagonal metric allowing for off-diagonal components that mix different spatial directions:

$$ds^2 = G_{MN} dx^M dx^N, \quad (3)$$

where the metric components G_{MN} are functions of the spatial coordinates, x_i , but independent of the time coordinate, x_0 .

The string propagation in such background is governed by the Nambu–Goto action

$$S_{\text{NG}} = \frac{1}{2\pi\alpha'} \int d\tau d\sigma \sqrt{-g}. \quad (4)$$

Here, $1/2\pi\alpha'$ is the string tension coefficient, $\alpha' = \ell_s^2$ is the Regge slope parameter and the fundamental string length scale ℓ_s , and g is the determinant of the induced metric on the world sheet. Parameterizing the string world sheet by the coordinates pair (τ, σ) , one then needs to find the induced metric tensor $g_{\alpha\beta}$, which is defined as

$$g_{\alpha\beta} = G_{MN} \partial_\alpha X^M \partial_\beta X^N \quad (5)$$

with the embedded coordinates X^M and components of the spacetime metric G_{MN} .

We employ a static gauge choice for the string world sheet, parameterizing it such that the time coordinate on the world sheet, τ , is identified with the background time x_0 . The spatial coordinate on the string world sheet, σ , is identified with a specific spatial direction in the global spacetime, x_p . The remaining coordinates, x_i with $i \neq 0, p$, are the dynamical fields $x_i(\sigma)$, describing how the string bends away from the straight line along σ . This configuration looks as follows:

$$x_0 = \tau, \quad x_p = \sigma, \quad x_i = x_i(\sigma), \quad (6)$$

$$x_i(\sigma = -L/2) = x_i(\sigma = +L/2) = x_{i_{\text{max}}}, \quad (7)$$

where the string endpoints are fixed at $\sigma = \pm L/2$ and $x_i = x_{i_{\text{max}}}$. Hence, the distance between endpoints in terms of σ has a simple form:

$$L = \int_{-L/2}^{L/2} d\sigma. \quad (8)$$

The Equations of Motion

The explicit view of the induced metric (5) in the terms of the background metric components (3) is

$$g_{\tau\tau} = G_{00}, \quad (9)$$

$$g_{\sigma\sigma} = G_{pp} + 2 \sum_i G_{pi} x'_i + \sum_i \sum_j G_{ij} x'_i x'_j, \quad (10)$$

$$g_{\tau\sigma} = g_{\sigma\tau} = G_{p0} + \sum_i G_{0i} x'_i, \quad (11)$$

where we denoted $x'_i = \frac{dx_i}{d\sigma}$. Using (9)–(11) one can write down the Lagrangian density as

$$\mathcal{L} = \sqrt{-g} = \sqrt{g_{\tau\sigma}^2 - g_{\tau\tau} g_{\sigma\sigma}} = \sqrt{-g_p - \sum_i x'_i \left[2h_{pi} + G_{00} \sum_j G_{ij} x'_j \right] + \left(\sum_i G_{0i} x'_i \right)^2}. \quad (12)$$

Here, we introduced following geometrical objects, which are the base terms in our work:

$$h_{ab} = G_{00} G_{ab} - G_{0a} G_{0b}, \quad (13)$$

$$g_a = h_{aa} = G_{00} G_{aa} - G_{0a}^2. \quad (14)$$

Quantity (13) characterizes a geometric coupling between directions a and b as seen by the string world sheet. For $a = b$, Eq. (14) is the world sheet metric determinant for a string oriented purely along the a -direction. Hence, g_p in (12) defines the geometry of the background spacetime swept by the unperturbed static string oriented along the p -direction. When $a \neq b$, h_{ab} describes how motions in directions a and b couple in the string dynamics, so h_{pi} in (12) reflects a geometrical connection between x_p and x_i directions. More precisely, h_{ab} is a projection metric on the spatial sections with $x_0 = \text{const}$, that will be discussed later.

Using (12), we find a first integral of the equations of motion (EoM), which corresponds to the conserved Hamiltonian density:

$$\mathcal{H} = \sum_i \mathcal{P}_i x'_i - \mathcal{L} = \frac{g_p + \sum_i h_{pi} x'_i}{\mathcal{L}} = \mathcal{C}, \quad (15)$$

where the quantities

$$\mathcal{P}_i = \frac{\partial \mathcal{L}}{\partial x'_i} = -\frac{h_{pi} + G_{00} \sum_j G_{ij} x'_j - G_{0i} \sum_j G_{0j} x'_j}{\mathcal{L}} \quad (16)$$

are the canonical momenta. The constant \mathcal{C} is fixed by the boundary condition at the string turning point, where all the coordinate derivatives vanish: $x'_i \Big|_{x_i=x_{i\min}} = 0$. Substituting this condition into (15) and solving for \mathcal{C} yields:

$$\mathcal{C} = -\sqrt{-g_p} \Big|_{x_i=x_{i\min}} = -\sqrt{G_{0p}^2 - G_{00} G_{pp}} \Big|_{x_i=x_{i\min}}. \quad (17)$$

One finds that the canonical momenta in Eq. (16), evaluated at the string turning point, are constant:

$$\mathcal{P}_i \Big|_{x_i=x_{i\min}} = -\frac{h_{pi}}{\sqrt{-g_p}} \Big|_{x_i=x_{i\min}} = \frac{1}{\mathcal{C}} h_{pi} \Big|_{x_i=x_{i\min}}. \quad (18)$$

These vanish for spacetimes with certain symmetries satisfying $h_{pi} = 0$ (the simplest case is the diagonal metric).

Now it's convenient to split coordinates x_i into radial x_r and transverse x_i ($i \neq r$) directions to change the integration variable σ to x_r via $d\sigma = dx_r/x'_r$. To solve for the derivative x'_r , we begin by squaring both sides of Eq. (15) to eliminate the square root present in the Lagrangian \mathcal{L} :

$$\frac{(g_p^{(T)})^2 + 2g_p^{(T)} h_{pr} x'_r + h_{pr}^2 x'^2_r}{\mathcal{L}_T^2 - g_r x'^2_r - 2x'_r \left[h_{pr} - G_{0r} \sum_{i \neq r} G_{0i} x'_i \right]} = \mathcal{C}^2,$$

where we defined

$$g_r = h_{rr} = G_{00} G_{rr} - G_{0r}^2, \quad (19)$$

$$g_p^{(T)} = g_p + \sum_{i \neq r} h_{pi} x'_i, \quad (20)$$

$$\mathcal{L}_T^2 = \mathcal{L}^2 \Big|_{x'_r=0} = -g_p - \sum_{i \neq r} x'_i \left[2h_{pi} + G_{00} \sum_{j \neq r} G_{ij} x'_j \right] + \left(\sum_{i \neq r} G_{0i} x'_i \right)^2. \quad (21)$$

Here, \mathcal{L}_T is the Lagrangian density for a purely transverse string profile with $x'_r = 0$, $g_p^{(T)}$ is a modification of (14) that takes into account the transverse corrections of the string shape, g_r is the determinant of the induced metric for a string oriented purely along the radial direction.

Then, by collecting terms with the same powers of x'_r , we obtain a quadratic equation:

$$ax'^2_r + bx'_r + c = 0 \quad (22)$$

with following coefficients

$$\begin{aligned} a &= h_{pr}^2 + \mathcal{C}^2 g_r, \\ b &= 2 \left[g_p^{(T)} h_{pr} + \mathcal{C}^2 \left(h_{pr} - G_{0r} \sum_{i \neq r} G_{0i} x'_i \right) \right], \\ c &= (g_p^{(T)})^2 - \mathcal{C}^2 \mathcal{L}_T^2. \end{aligned}$$

The solution of Eq. (22) is given by a standard expression:

$$x'_r = \frac{-b \pm \sqrt{b^2 - 4ac}}{2a}. \quad (23)$$

For instance, in the backgrounds family with $h_{pr} = 0$ for string configurations with simple transverse shape $x'_i = 0$ the general expression for x'_r simplifies to

$$x'^2_r = -\frac{g_p(g_p + \mathcal{C}^2)}{\mathcal{C}^2 g_r}, \quad (24)$$

while considering of diagonal metrics leads to

$$x'^2_r = -\frac{G_{pp}(G_{00}G_{pp} + \mathcal{C}^2)}{\mathcal{C}^2 G_{rr}}. \quad (25)$$

Possible source of the parity violation

For arbitrary stationary background $h_{pr} \neq 0$, so a consideration of the simple string ansatz with $x'_i = 0$ leads to the following view of EoM (23):

$$x'_r = \frac{\sqrt{g_p + \mathcal{C}^2}}{h_{pr}^2 + \mathcal{C}^2 g_r} \left(-h_{pr} \sqrt{g_p + \mathcal{C}^2} \pm |\mathcal{C}| \sqrt{-h} \right), \quad (26)$$

where we defined $h = -(h_{pr}^2 - g_r g_p) = -(h_{pr}^2 - h_{rr} h_{pp})$, the meaning of which we will find below. Note that the equation (26) is generally non-symmetric with respect to the string turning point. Hence, a non-zero value of the quantity h_{pr} signals a breakdown of spatial parity symmetry along the involved directions.

As we noted earlier, h_{pr} reflects space asymmetry in the $p - r$ plane. The physical meaning of h becomes especially clear when the stationary metric is written in the standard form with splitting along the timelike Killing field:

$$ds^2 = G_{00}(dt + A_a dx^a)^2 + \frac{h_{ab}}{G_{00}} dx^a dx^b, \quad (27)$$

where G_{00} is the norm of the time-like Killing field, $A_a = G_{0a}/G_{00}$ is the gravitomagnetic potential, so h_{pr} defines the geometry of the spatial sections. Hence,

$$h = -(h_{pr}^2 - h_{rr} h_{pp}) = \det \begin{pmatrix} h_{pp} & h_{pr} \\ h_{pr} & h_{rr} \end{pmatrix} = G_{00} \det \begin{pmatrix} G_{00} & G_{0p} & G_{0r} \\ G_{0p} & G_{pp} & G_{pr} \\ G_{0r} & G_{pr} & G_{rr} \end{pmatrix}, \quad (28)$$

so is the determinant of the projection metric on spatial sections with $x_0 = t = \text{const}$. In the parametrization (27), h_{pr} combines two possible sources of parity violation: non-zero off-diagonal metric element $G_{pr} \neq 0$ and the presence of gravitomagnetic fields $A_p \neq 0$, $A_r \neq 0$. For instance, it may correspond to pseudoscalar condensates or some stationary flows.

Consequently, the asymmetry of the string profile, the source of which is $h_{pr} \neq 0$, probes the parity violation. A quantitative measure of this violation can be provided by the shift of the string turning point away from the midpoint between the quark and antiquark, which is computed from the first integral of the equations of motion. When $h_{pr} = 0$, the profile becomes symmetric, however, this condition does not necessarily restore full parity invariance of the background: it may merely reflect a specific compensation or a configuration that is insensitive to the existing symmetry violations. Moreover, one be mindful that h_{pr} is not a diffeomorphism-invariant scalar: its non-zero value in the chosen parametrization signals parity violation, but the invariant physical content of the latter should be extracted from appropriate curvature invariants or conserved quantities.

General expression for the static potential

Expressing \mathcal{L} via \mathcal{C} from (15), one can simplify the action (4):

$$S_{\text{NG}} = \frac{\mathcal{T}}{2\pi\alpha'\mathcal{C}} \int_{-L/2}^{L/2} d\sigma \left(g_p^{(T)} + h_{pr} x'_r \right). \quad (29)$$

Taking into account that the EoM (26) generally is not symmetric with respect to the string turning point $x_{r_{\min}}$, we rewrite expressions (8) and (29) as

$$L = \int_{x_{r_{\min}}}^{x_{r_{\max}}} dx_r \left(\frac{1}{x'_{r_+}} + \frac{1}{x'_{r_-}} \right), \quad (30)$$

$$S_{\text{NG}} = \frac{\mathcal{T}}{2\pi\alpha'\mathcal{C}} \left[\int_{x_{r_{\min}}}^{x_{r_{\max}}} dx_r \left(\frac{g_p^{(T)}}{x'_{r_+}} + \frac{g_p^{(T)}}{x'_{r_-}} + 2h_{pr} \right) \right], \quad (31)$$

where we denoted two different branches by $x_{r\pm}$.

The Nambu–Goto action (31) typically exhibits divergence that requires renormalization. For asymptotically AdS spaces (and other geometries with similar ultraviolet behavior) this is accomplished by subtracting the action of two straight, disconnected strings extending from the boundary to the deep infrared:

$$S_0 = \frac{\mathcal{T}}{\pi\alpha'} \int_{x_{r_0}}^{x_{r_{\max}}} dx_r \sqrt{-g_r} = \frac{\mathcal{T}}{\pi\alpha'} \left(\int_{x_{r_0}}^{x_{r_{\min}}} + \int_{x_{r_{\min}}}^{x_{r_{\max}}} \right) dx_r \sqrt{-g_r}, \quad (32)$$

with g_r is defined in equation (19), and x_{r_0} denotes the infrared endpoint: either a horizon radius or, in horizon-free geometries, the deep bulk limit. Hence, the following expression for the renormalized action can be obtained:

$$S_{\text{NG}}^{\text{ren}} = S_{\text{NG}} - S_0 = \frac{\mathcal{T}}{\pi\alpha'} \left[\frac{1}{2\mathcal{C}} \int_{x_{r_{\min}}}^{x_{r_{\max}}} dx_r \left(\frac{g_p^{(T)}}{x'_{r_+}} + \frac{g_p^{(T)}}{x'_{r_-}} + 2h_{pr} - 2\mathcal{C}\sqrt{-g_r} \right) - \int_{x_{r_0}}^{x_{r_{\min}}} dx_r \sqrt{-g_r} \right]. \quad (33)$$

Finally, associating the string with a heavy quark-antiquark pair, the static potential energy (2) can be explicitly written as

$$\pi\alpha'V = \frac{1}{2\mathcal{C}} \int_{x_{r_{\min}}}^{x_{r_{\max}}} dx_r \left(\frac{g_p^{(T)}}{x'_{r_+}} + \frac{g_p^{(T)}}{x'_{r_-}} + 2h_{pr} - 2\mathcal{C}\sqrt{-g_r} \right) - \int_{x_{r_0}}^{x_{r_{\min}}} dx_r \sqrt{-g_r}, \quad (34)$$

which is a general expression obtained within the string theory for a general static string configuration in arbitrary stationary D -dimensional background. The obtained result does not depend on whether one works within the framework of the holographic models, or effective description of the static QCD fields between a heavy quark pair.

Note that without additional assumptions, confident simplifications of (34) are not justified. For example, while one may postulate string symmetry about the string turning point $x_{r_{\min}}$, such a symmetric profile may not represent the minimum-energy configuration when the metric coupling h_{pr} is non-zero (see Eq. (26) and discussions later). Although symmetric solutions might exist in special cases even for $h_{pr} \neq 0$, rigorous confidence in this symmetry requires $h_{pr} = 0$.

Isolation of the linear-in-distance term for some background families

It is easy to see that the general formulas (30) and (34) are reduced to particular cases obtained in the literature earlier. For instance, for diagonal metrics with account of (25) it simplifies to

$$L = 2|\mathcal{C}| \int_{x_{r_{\min}}}^{x_{r_{\max}}} dx_r \sqrt{-G_{00}G_{rr}} \frac{1}{\sqrt{G_{00}G_{pp}(G_{00}G_{pp} + \mathcal{C}^2)}} \quad (35)$$

$$V = \frac{1}{\pi\alpha'} \left[\int_{x_{r_{\min}}}^{x_{r_{\max}}} dx_r \sqrt{-G_{00}G_{rr}} \left(\frac{\sqrt{G_{00}G_{pp}}}{\sqrt{G_{00}G_{pp} + \mathcal{C}^2}} - 1 \right) - \int_{x_{r_0}}^{x_{r_{\min}}} dx_r \sqrt{-G_{00}G_{rr}} \right] \quad (36)$$

$$= \frac{1}{\pi\alpha'} \left[-\frac{\mathcal{C}L}{2} + \int_{x_{r_{\min}}}^{x_{r_{\max}}} dx_r \sqrt{-G_{00}G_{rr}} \left(\sqrt{1 + \frac{\mathcal{C}^2}{G_{00}G_{pp}}} - 1 \right) - \int_{x_{r_0}}^{x_{r_{\min}}} dx_r \sqrt{-G_{00}G_{rr}} \right], \quad (37)$$

where we used the following identity:

$$\frac{x}{\sqrt{x^2 + 1}} = \frac{\sqrt{x^2 + 1}}{x} - \frac{1}{x\sqrt{x^2 + 1}} \quad (38)$$

The equation (37) is exactly the same obtained in [138], taking into account a relation between the constants definitions ($\mathcal{C} = -c$).

For the Schwarzschild-AdS₅ and Kerr-AdS₅ black holes considered in [205] we also receive the same expressions (see Eqs. (3.12) and (3.32) in [205]). In fact, these black holes solutions are the members of the backgrounds family with $h_{pr} = 0$, and for the string configurations with fixed transverse shape $x'_i = 0$ we can isolate the linear part in the potential using (24) and (38):

$$L = 2|\mathcal{C}| \int_{x_{r_{\min}}}^{x_{r_{\max}}} dx_r \sqrt{-g_r} \frac{1}{\sqrt{g_p(g_p + \mathcal{C}^2)}} \quad (39)$$

$$V = \frac{1}{\pi\alpha'} \left[\int_{x_{r_{\min}}}^{x_{r_{\max}}} dx_r \sqrt{-g_r} \left(\frac{\sqrt{g_p}}{\sqrt{g_p + \mathcal{C}^2}} - 1 \right) - \int_{x_{r_0}}^{x_{r_{\min}}} dx_r \sqrt{-g_r} \right] \quad (40)$$

$$= \frac{1}{\pi\alpha'} \left[-\frac{\mathcal{C}L}{2} + \int_{x_{r_{\min}}}^{x_{r_{\max}}} dx_r \sqrt{-g_r} \left(\sqrt{1 + \frac{\mathcal{C}^2}{g_p}} - 1 \right) - \int_{x_{r_0}}^{x_{r_{\min}}} dx_r \sqrt{-g_r} \right]. \quad (41)$$

The result (41) also means that for such backgrounds (with $h_{pr} = 0$) the Nambu–Goto action for a simple static symmetric string configuration ($x'_i = 0$, $x'_r \neq 0$) can be initially written as:

$$S_{\text{NG}} = \frac{\mathcal{T}}{\pi\alpha'} \left(-\frac{\mathcal{C}L}{2} + \int_{x_{r_{\min}}}^{x_{r_{\max}}} dx_r \sqrt{-g_r} \sqrt{1 + \frac{\mathcal{C}^2}{g_p}} \right) \quad (42)$$

with \mathcal{C} and L defined in (17) and (39), correspondingly.

III. THE QUARK-ANTIQUARK POTENTIAL IN THE THE RINDLER-ADS SPACE

The Rindler-AdS background

Continuing our previous work [205] on the analysis of the influence of rotation on the confinement-deconfinement phase transition within the holographic framework, in this section we will clarify the influence of acceleration. Within the AdS/CFT correspondence, one need to consider the Rindler-AdS space, the dual of which is the $\mathcal{N} = 4$ super Yang-Mills theory. The Rindler-AdS spacetime has been widely investigated in [223, 229, 232, 235, 245].

The Rindler-AdS metric is given by the following expression:

$$ds^2 = -a_c^2 \xi^2 dt^2 + \frac{d\xi^2}{1 + a_c^2 \xi^2} + (1 + a_c^2 \xi^2) \left[d\chi^2 + \frac{1}{a_c^2} \sinh^2(a_c \chi) d\Omega_{d-2}^2 \right]. \quad (43)$$

For a qualitative analysis, one often sets the coordinate Rindler acceleration equal to the inverse AdS radius, $a_c = 1/\mathcal{R}$ (see, for instance, Ref. [235]). The numerical value of a_c itself is not a physical invariant (it can be changed by rescaling the coordinates), but the AdS radius \mathcal{R} provides the intrinsic geometric scale of the spacetime. The quantity $a_c = 1/\mathcal{R}$ then carries the correct dimension of acceleration and serves as a natural reference value.

In the limit $a_c \xi \rightarrow 0$ the metric (43) reduces to the line element of flat Rindler space with a horizon at $\xi = 0$:

$$ds^2 = -a_c^2 \xi^2 dt^2 + d\xi^2 + d\chi^2 + \chi^2 d\Omega_{d-2}^2. \quad (44)$$

The coordinates (43) describe a region satisfying $(X^1)^2 - (X^0)^2 > 0$ and $(X^1)^2 - (X^{d+1})^2 > 0$ in a $(d+2)$ -dimensional embedding Minkowski space with two time-like directions:

$$-(X^0)^2 + (X^1)^2 + \dots + (X^d)^2 - (X^{d+1})^2 = -\mathcal{R}^2, \quad (45)$$

which possesses the symmetry group $O(2, d)$, corresponding to AdS_{d+1}. This embedding shows that the Rindler observers in AdS follow hyperbolic trajectories in the ambient Minkowski space, i.e., they are also Rindler observers with respect to the embedding space.

At $\xi \rightarrow \infty$ the metric (43) asymptotically approaches the conformal boundary of AdS:

$$ds_{\text{boundary}}^2 = -dt^2 + d\chi^2 + \frac{1}{a_c^2} \sinh^2(a_c \chi) d\Omega_{d-2}^2, \quad (46)$$

which is the metric on $\mathbb{R} \times \mathbb{H}^{d-1}$, where the hyperbolic spatial section \mathbb{H}^{d-1} has a curvature radius of $1/a_c = \mathcal{R}$. Moreover, for any finite ξ , the induced metric on a constant- ξ hypersurface is also conformally equivalent to $\mathbb{R} \times \mathbb{H}^{d-1}$. This reflects the fact that the Rindler-AdS foliation preserves the conformal structure of the boundary at every finite ξ , even though the holographic dual CFT in the AdS/CFT sense is usually defined only on the ideal conformal boundary attached at $\xi \rightarrow \infty$.

As it is known from the general relativity, the temperature seen by an observer moving with constant acceleration is not always proportional to the proper acceleration. For the Rindler-AdS space the proper acceleration of an observer at constant ξ is given by

$$a_{\text{prop}}^2 = a_{\text{loc}}^2 + a_c^2 = \frac{1}{\xi^2} + \frac{1}{\mathcal{R}^2}, \quad (47)$$

where the local acceleration is defined as $a_{\text{loc}} = \frac{1}{\xi}$. In work [223] a general formula for the local temperature in (A)dS_{d+1} was obtained:

$$T_{\text{loc}} = \frac{1}{2\pi} \sqrt{\frac{2\Lambda}{d(d-1)} + a_{\text{prop}}^2} = \frac{a_{\text{embed}}}{2\pi}, \quad (48)$$

where a_{embed} is the proper acceleration of the Rindler observer in the flat embedding space and Λ is the cosmological constant.

For AdS_{d+1} the cosmological constant looks as $\Lambda = -\frac{1}{\mathcal{R}^2} \frac{d(d-1)}{2}$, therefore the condition for a real value of the temperature requires the proper acceleration to satisfy $a_{\text{prop}} \geq \frac{1}{\mathcal{R}} = a_{\text{crit}}$, where we defined a critical acceleration a_{crit} . The observers with $a_{\text{prop}} > a_{\text{crit}}$ possess a non-degenerate Rindler-type horizon and measure a non-zero local temperature (48), which can be rewritten as

$$T(\xi) = T_{\text{loc}} = \frac{1}{2\pi} \sqrt{a_{\text{prop}}^2 - a_{\text{crit}}^2}. \quad (49)$$

At $a_{\text{prop}} = a_{\text{crit}}$ the horizon becomes extremal (zero surface gravity) and the local temperature vanishes. As an example, such observer is located at $\xi \rightarrow \infty$. Finally, observers with $a_{\text{prop}} < a_{\text{crit}}$ have no causal horizon. Their trajectories are globally extendible and they do not perceive a thermal spectrum.

Remarkably, the critical acceleration coincides exactly with the parameter that appears in the Rindler-AdS metric (43), i.e. $a_{\text{crit}} = a_c$. The proper acceleration (47) is always greater than or equal to a_c . Thus, the Rindler-AdS coordinate system naturally covers only the worldlines of super-critical (and, asymptotically, critical) observers. The parameter a_c in the metric therefore has a clear physical interpretation: it sets both the AdS curvature scale \mathcal{R} and the minimal acceleration required for an observer to possess a horizon and a well-defined temperature in AdS.

Using (47), one can obtain a final expression for the local temperature:

$$T(\xi) = T_{\text{loc}} = \frac{1}{2\pi\xi}. \quad (50)$$

Remarkably, this is precisely the same expression as for an accelerated detector in flat Rindler space, despite the non-zero curvature of AdS. The horizon at $\xi = 0$ possesses a Hawking temperature T_H , defined via its surface gravity. For the Rindler-AdS metric, one finds $T_H = a_c/(2\pi) = 1/(2\pi\mathcal{R})$, so the local temperature (50) can then be written as

$$T(\xi) = \frac{T_H}{\sqrt{-G_{tt}(\xi)}} = \frac{1}{2\pi\xi}, \quad (51)$$

which is exactly the Tolman-Ehrenfest law for temperature distribution in a static gravitational field. Thus, while the horizon itself has a fixed temperature T_H , an accelerated observer at finite ξ experiences a higher local temperature due to gravitational redshift.

Influence of the acceleration on the static quark-antiquark potential

Choosing the following string ansatz,

$$\tau = t, \quad \sigma = \chi, \quad \xi = \xi(\sigma), \quad \xi(\sigma = \pm L/2) = \xi_{\text{max}} = \infty, \quad (52)$$

one can find our main quantities for the potential and distance expressions:

$$g_p = G_{tt}G_{\chi\chi} = -a^2\xi^2(1+a^2\xi^2), \quad (53)$$

$$g_r = G_{tt}G_{\xi\xi} = -\frac{a^2\xi^2}{1+a^2\xi^2}. \quad (54)$$

The first integral takes the following value

$$\mathcal{C} = -a\xi_m\sqrt{1+a^2\xi_m^2}, \quad (55)$$

where the physical value of the string turning point, ξ_m , satisfying $\xi \geq 0$, $\mathcal{C}^2 \geq 0$, $a > 0$, is given by

$$\xi_m = \frac{\sqrt{\sqrt{4\mathcal{C}^2 + 1} - 1}}{\sqrt{2}a}. \quad (56)$$

In the special case of an acceleration $a = 1/\xi_m$, the first integral is a universal constant $\mathcal{C} = -\sqrt{2}$.

Now, using (53)-(56) one can analytically calculate the integrals in the expressions for the distance (39) and potential (41) between quarks. Direct calculations (see Appendix A for details) lead to the following expressions for the distance L and potential V :

$$L = 2\xi_m \operatorname{Re} \left[\tilde{\Pi}(n, m) - \frac{K(1-m)}{1-n} \right], \quad (57)$$

$$\pi\alpha'V = \frac{1}{a} + \sqrt{\frac{1}{a^2} + \xi_m^2} \operatorname{Re}[iK(m) - \tilde{E}(m)] \quad (58)$$

$$= \frac{1}{a} - \frac{\mathcal{C}L}{2} + \frac{\xi_m\mathcal{C}}{n} \operatorname{Re}[\tilde{K}(m) - n\tilde{\Pi}(n, m) - \tilde{E}(m)], \quad (59)$$

where we introduced linear combinations of the complete elliptic integrals

$$\tilde{\Pi}(n, m) = m\Pi(1-n, 1-m) + i\Pi(n, m), \quad (60)$$

$$\tilde{K}(m) = mK(1-m) + iK(m), \quad (61)$$

$$\tilde{E}(m) = E(1-m) + iE(m) \quad (62)$$

with the characteristic n , elliptic modulus k and parameter m given by

$$n = -a^2\xi_m^2, \quad m = k^2 = \frac{n}{1-n}. \quad (63)$$

It was tested that the expressions (57)-(59) give the same result as direct numerical integrations of (57) and (41) in the Rindler-AdS case. Notably, the elliptic integrals in the context of the static interquark potential are also arisen in different setups, for instance [247, 248].

To compare different AdS geometries (different radii \mathcal{R}) while keeping a fixed reference length ℓ , it is convenient to introduce a dimensionless scaling parameter a_0 via the relation $a_c = a_0/\ell$, where ℓ is a fixed reference length, for example the AdS radius of a chosen "reference" geometry (so that $a_0 = 1$ in that case). This parametrization emphasizes that, when ℓ is held fixed, the dimensionless number a_0 distinguishes one geometry from another, whereas a_c (or equivalently $1/\mathcal{R}$) absorbs the dimensional dependence.

Consequently, physical observables should depend on acceleration only through dimensionless combinations. For example, in the final part of this section we will see that the quark-antiquark potential, written as dimensionless function, $a_c V$, of the dimensionless distance between quarks, $a_c L$, is independent of the specific numerical choice of a_0 , which is a direct consequence of scale invariance in the Rindler-AdS background. On the other hand, the dimensionless ratio V/ℓ expressed as a function of L/ℓ retains an explicit dependence on a_0 , thereby reflecting how the underlying geometry changes with the rescaled acceleration parameter.

We show dependencies of the potential and distance between quarks in the Rindler-AdS background at in Fig. 1 for several values of the acceleration parameter $a_0 = a\ell = 0.4, 0.6, 1, 2$. To avoid dimensions we express all the quantities in terms of ℓ . Also the potential is multiplied by $\pi\alpha'$ to keep arbitrariness of α' .

There are two branches of the potential, of which the upper one is unphysical. Beyond some critical distance, where the potential energy of our string configuration equals that of a free quark pair, our string ansatz is no longer energetically favorable and the confinement-deconfinement phase transition occurs. It happens at a special relation

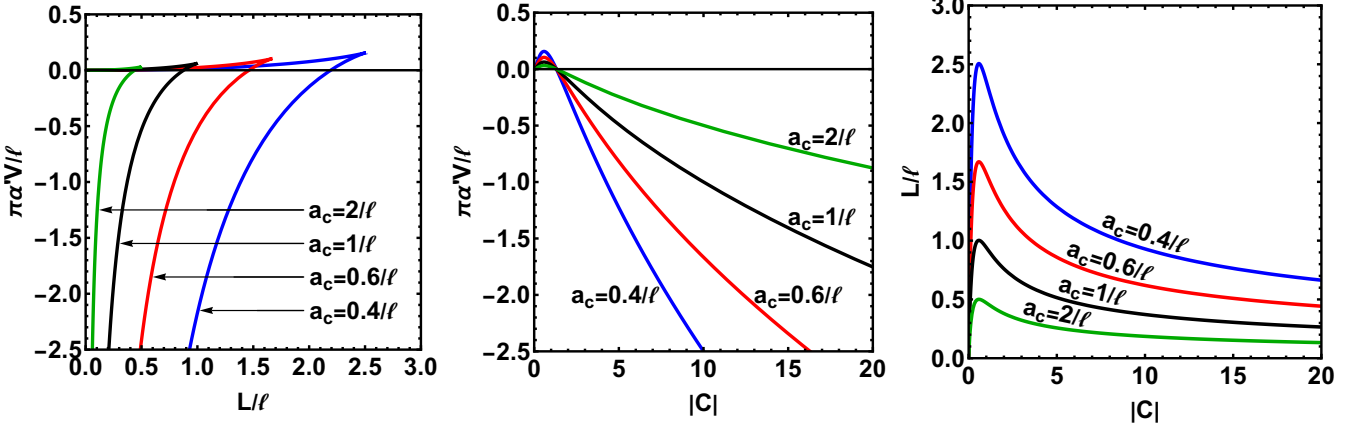


FIG. 1. Numerical calculations in the Rindler-AdS background (43) for (1) the quark-antiquark potential V (41) depending on the distance L (39) between quarks; (2) the potential V as a function of the absolute value of constant C ; (3) the distance L as a function of the absolute value of constant C . Different line colors correspond to different values of the acceleration: blue for $a = 0.4/\ell$, red for $a = 0.6/\ell$, black for $a = 1/\ell$, and green for $a = 2/\ell$.

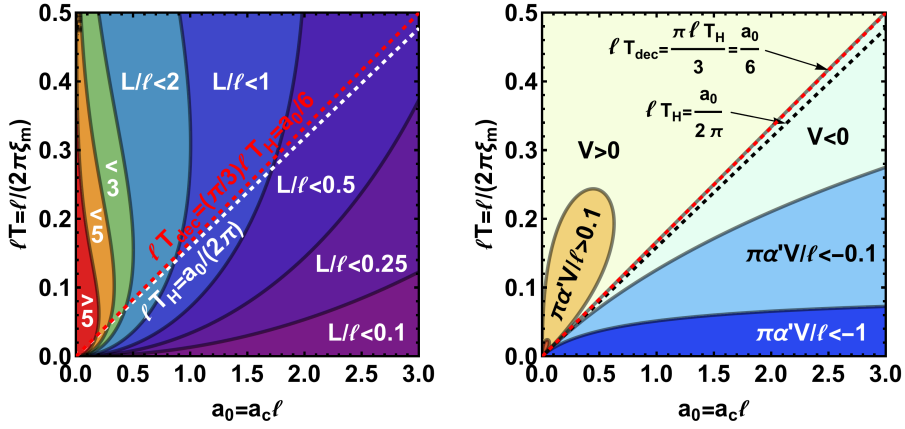


FIG. 2. Contours plots of the distance L (first pane) and potential V (second pane) between quarks as functions of the dimensionless acceleration parameter $a_0 = a_c \ell$ and of the dimensionless temperature at the string turning point $\ell T = \ell/(2\pi\xi_m)$. Different values of V or L , corresponding certain contours, are depicted by colors and labels. The critical temperature $T_{\text{dec}} = (\pi/3)T_H = a_c/6$ of the phase transition is shown by a red dashed line, while the Hawking temperature T_H is drawn by a rest dashed line.

between the position of the string turning point ξ_m and the value of the acceleration a_c (or the AdS radius \mathcal{R}). Namely, it happens at $\xi_m = 3/(\pi a_c) = 3\mathcal{R}/\pi$ with temperature $T_{\text{dec}} = (\pi/3)T_H = a_c/6$, that is depicted by a red dashed line in the contour plots in Fig. 2. Note that it is slightly higher (the factor is ≈ 1.05) than the horizon temperature T_H , which is depicted by a second dashed line in Fig. 2.

In Fig. 3 we also shown 3-dimensional plots of the distance and potential in the acceleration-temperature at the string turning point plane. As one can see, at low acceleration a_0 and temperatures $T(\xi_m)$ the distance and potential undergo faster growth and diverge in the limit of $a_c \rightarrow 0$ and $T(\xi_m) \rightarrow 0$.

An accelerated observer in a Rindler wedge has access only to the part of spacetime limited by its horizon. As acceleration increases, the observer moves closer to the horizon. Two accelerated quarks, in order to remain in causal connection with each other, must be closer to each other, otherwise the horizon will break the string between them. The critical distance at which the string can exist decreases with increasing acceleration, see Fig. 1. The shorter string is in a more "compressed" state. The energy stored in the string per unit length (tension) is constant, but due to the curvature of spacetime and the horizon influence, the effective energy that must be expended to separate the quarks increases. This manifests itself as an increase in the interquark potential, which can be seen in Fig. 1.

Hence, the phase transition temperature increases with the acceleration $a_c = a_0/\ell = 1/\mathcal{R}$. This occurs either by increasing the dimensionless parameter a_0 at fixed curvature scale ℓ , or by decreasing ℓ at fixed a_0 , which is the same as the AdS horizon \mathcal{R} decrease. Qualitatively, our results are in an agreement with the ones obtained by other

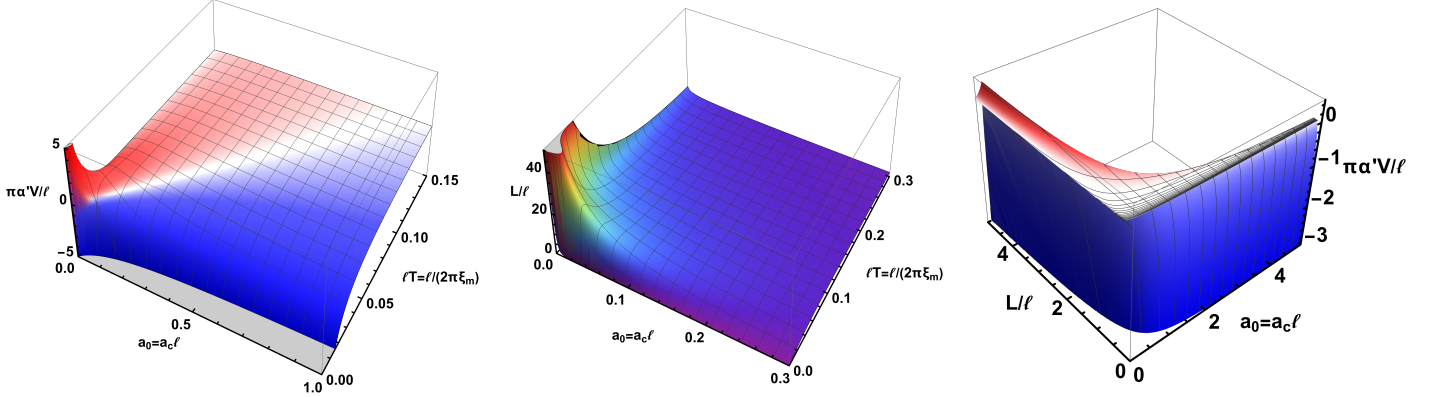


FIG. 3. 3-dimensional plots of the distance L (first pane) and potential V (second pane) between quarks as functions of the dimensionless acceleration parameter $a_0 = a_c \ell$ and of the dimensionless temperature at the string turning point $\ell T = \ell/(2\pi\xi_m)$; the potential V as a function of the distance L and acceleration parameter a_0 (third pane).

authors, for example in the works [94, 103].

However, one can argue that our system is scale invariant, so a certain value of the acceleration parameter a_c sets only the scale between time and space coordinates. One can perform a transformation of the coordinates in the Rindler-AdS metric (43) and redefine the originally chosen acceleration value a_c to another value or even get rid of the acceleration by the coordinate transformation $\tilde{x}_i = a_c x_i$.

Indeed, the potential scaled onto acceleration value, $\tilde{V} = a_c V$, as a function of the acceleration-scaled distance, $\tilde{L} = a_c L$, shows no dependence on the certain acceleration value a_c , see Fig. 4. In such terms the Hawking temperature is a universal constant $\tilde{T}_H = 1/2\pi$, which does not depend on the acceleration or AdS radius values. Hence, one have the phase transition temperature is also constant: $\tilde{T}_{dec} = (\pi/3)\tilde{T}_H = 1/6$. This universality reflects the scale invariance and self-similarity of our holographic setup. Interestingly, the factor 1/6 is also relates entropy of the free field CFT and the Rindler horizon [235], $S_{\text{CFT}} = S_{\text{Rindler}}/6$, but it may be a coincidence.

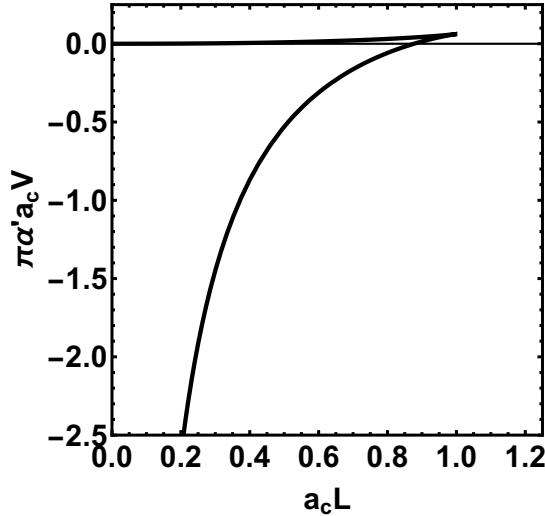


FIG. 4. The scaled onto acceleration potential $\tilde{V} = a_c V$ as a function of the acceleration-scaled distance $\tilde{L} = a_c L$.

IV. SUMMARY AND DISCUSSION

In this paper, we have presented the calculations of the static heavy quark-antiquark potential within the string theory for an arbitrary stationary background. We established that for a simple U-shaped string with only radial dependence on the space string coordinate, $x'_r(\sigma) \neq 0$, the string is generally not symmetric about its turning point, and the symmetry (at least for the EoM) restores only for backgrounds with $h_{pr} = G_{00}G_{pr} - G_{0p}G_{0r} = 0$.

Consequently, such asymmetric strings directly probe a possibility of the parity violation in the quark-antiquark interaction. Nevertheless, we obtained a general expression (34) for the static potential within a non-symmetric string profile.

Then, we shown that for a simple string configuration (only radial dependency $x'_i = 0$, $x'_r \neq 0$ and symmetry with respect to the turning point) one can directly isolate a linear-in-distance term even for complicated non-diagonal metrics with the only one constraint ($h_{pr} = G_{00}G_{pr} - G_{0p}G_{0r} = 0$), see Eq. (41). It is a wide class of the backgrounds, including simple diagonal (or semi-diagonal with respect to p and r as for the AdS family solutions) cases, stationary metrics, special cases with $G_{pr} = \frac{G_{0p}G_{0r}}{G_{00}}$, where one can diagonalize this metric part by a simple time shift depending on r and p , etc. It also means that one can initially work with simplified version of the Nambu–Goto action, expressed in terms of the first integral and the distance between string endpoints (quarks), see (42).

In the second part of the work, within the framework of the holographic duality between the Rindler-AdS space and the accelerated $\mathcal{N} = 4$ super Yang-Mills plasma, we find analytic expressions for the distance (57) and static potential (58), (59) between quarks in terms of the elliptic integrals. We show that the distance between quarks decreases, the static potential between them increases, and the deconfinement phase transition temperature, $T_{\text{dec}} = (\pi/3)T_H = a_c/6$, increases with an acceleration, a_c .

However, we observe that an acceleration-scaled potential, $\tilde{V} = a_c V$, as a function of the acceleration-scaled distance, $\tilde{L} = a_c L$, does not depend on the certain value of the acceleration, a_c . This result, reflecting the scale invariance and self-similarity of the holographic setup, can be also obtained in the dimensionless metric after scaling of the coordinates onto the acceleration, $\tilde{x}_i = a_c x_i$, for which one obtains an universal value of the phase transition temperature, $\tilde{T}_{\text{dec}} = (\pi/3)\tilde{T}_H = 1/6$.

Finally, we want to note that the interquark potential has a similar dependence on the distance as in the case of the D -brane [131] and D -instanton [206] in the AdS space, the Schwarzschild-AdS and Kerr-AdS black holes [205], and other cases [137, 191, 207, 247]. Therefore, we can conclude that this is a common feature of the simple string ansatz (52) in the AdS-like backgrounds.

Appendix A: Analytic calculations in the Rindler-AdS background

First, inserting (53)-(56) into (39) leads to the following expression for the distance between string endpoints L :

$$\begin{aligned} L &= 2|\mathcal{C}| \int_{\xi_m}^{\infty} \frac{d\xi}{1 + a^2\xi^2} \frac{1}{\sqrt{a^2\xi^2(1 + a^2\xi^2) - \mathcal{C}^2}} \\ &= //x = a\xi; x_m = a\xi_m// = \frac{2|\mathcal{C}|}{a} \int_{a\xi_m}^{\infty} \frac{dx}{1 + x^2} \frac{1}{\sqrt{(x^2 - x_m^2)(x^2 + x_m^2 + 1)}} \\ &= //y = \frac{x}{x_m}; n = -x_m^2; m = k^2 = \frac{n}{1 - n}// = 2i\xi_m \int_1^{\infty} \frac{dy}{1 - ny^2} \frac{1}{\sqrt{(1 - y^2)(1 - my^2)}} \\ &= 2i\xi_m \Pi(\arcsin y; n, m) \Big|_{y=1}^{y \rightarrow \infty}, \end{aligned} \quad (\text{A.1})$$

where for clarity we shown auxiliary variable redefinitions inside the double slashes. Here we also introduced

$$\Pi(z; n, m) = \int_0^z dx \frac{1}{(1 - nx^2)\sqrt{(1 - x^2)(1 - mx^2)}}. \quad (\text{A.2})$$

$$\Pi(n, m) = \Pi(z = \pi/2; n, m), \quad (\text{A.3})$$

which are the incomplete and complete elliptic integrals of the third kind, correspondingly, with the characteristic n and elliptic modulus $k = \sqrt{m}$.

One can note that $n = -a^2\xi_m^2 < 0$ and $m = k^2 = n/(1 - n) < 0$, so the modulus k is complex-valued. While this representation is mathematically well-defined, the analytic continuation of elliptic integrals to complex parameters introduces branch ambiguities, so to avoid this problem we take the real part of the analytically continued expression. Using the identity for the asymptotic behavior of the elliptic integral of the third kind with imaginary argument,

$$\begin{aligned} \lim_{\alpha \rightarrow \infty} \Pi(-i\alpha; n, m) &= i \frac{F(-\pi/2; 1 - m) - n\Pi(-\pi/2; 1 - n, 1 - m)}{1 - n} \\ &= -i \frac{n\Pi(1 - n, 1 - m) - K(1 - m)}{1 - n}, \end{aligned} \quad (\text{A.4})$$

we can evaluate the upper limit explicitly. Substituting this into our expression for the proper length yields to

$$\begin{aligned} L &= 2\xi_m \operatorname{Re} \left[\frac{n\Pi(1-n, 1-m) - K(1-m)}{1-n} + i\Pi(n, m) \right] \\ &= 2\xi_m \operatorname{Re} \left[\tilde{\Pi}(n, m) - \frac{K(1-m)}{1-n} \right], \end{aligned} \quad (\text{A.5})$$

where we introduced the following shorthand notation:

$$\tilde{\Pi}(n, m) = m\Pi(1-n, 1-m) + i\Pi(n, m). \quad (\text{A.6})$$

Similarly, one can calculate an analytic formula for the potential. After direct substitution of (53)-(56) into (40) we obtain

$$\pi\alpha' V = \int_{\xi_m}^{\infty} d\xi \frac{a^2\xi^2}{\sqrt{\mathcal{C}^2 - a^2\xi^2(1 + a^2\xi^2)}} - \int_0^{\infty} d\xi \frac{a\xi}{\sqrt{1 + a^2\xi^2}},$$

where the calculations of the second integral is straightforward:

$$\int_0^{\infty} d\xi \frac{a\xi}{\sqrt{1 + a^2\xi^2}} = \sqrt{\frac{1}{a^2} + \xi^2} \Big|_{\xi=0}^{\xi \rightarrow \infty}. \quad (\text{A.7})$$

The first integral is calculated in a similar way as (A.1), namely

$$\begin{aligned} \int_{\xi_m}^{\infty} d\xi \frac{a^2\xi^2}{\sqrt{\mathcal{C}^2 - a^2\xi^2(1 + a^2\xi^2)}} &= \left\| y = \xi/\xi_m, \quad n = -a^2\xi_m^2, \quad m = k^2 = \frac{n}{1-n} \right\| \\ &= i\sqrt{\frac{1}{a^2} + \xi_m^2} \left[\int_1^{\infty} dy \frac{\sqrt{1-my^2}}{\sqrt{1-y^2}} - \int_1^{\infty} dy \frac{1}{\sqrt{(1-y^2)(1-my^2)}} \right] \\ &= i\sqrt{\frac{1}{a^2} + \xi_m^2} [E(\arcsin y; m) - F(\arcsin y; m)] \Big|_{y=1}^{y \rightarrow \infty}, \end{aligned}$$

where

$$F(z; m) = \int_0^z dx \frac{1}{\sqrt{(1-x^2)(1-mx^2)}}, \quad (\text{A.8})$$

$$E(z; m) = \int_0^z dx \frac{\sqrt{1-mx^2}}{\sqrt{1-x^2}} \quad (\text{A.9})$$

are the incomplete elliptic integrals of the first and second kind, correspondingly. In turn, at the lower bound $y = 1$ one come to the complete integrals of the first, $K(m)$, and second, $E(m)$, kinds:

$$K(m) = F(z = \pi/2; m), \quad (\text{A.10})$$

$$E(m) = E(z = \pi/2; m). \quad (\text{A.11})$$

At the upper integration bound $y \rightarrow \infty$ one can use the following limit for $F(z; m)$:

$$\lim_{y \rightarrow \infty} F(\arcsin y; m) = -iK(1-m), \quad (\text{A.12})$$

while for $E(z; m)$ one must explicitly perform the imaginary-argument transformation:

$$E(i\phi; m) = i \left(F(\psi; 1-m) - E(\psi; 1-m) + \tan \psi \sqrt{1 - (1-m)\sin^2 \psi} \right). \quad (\text{A.13})$$

At $y \rightarrow \infty$ the two first terms transform to the complete integrals with minus sign. The last term in (A.13) diverges in the same way as the upper bound in (A.7), so we can get rid of them both. Collecting (A.7)-(A.13), we come to the following formula for the potential:

$$\begin{aligned} \pi\alpha' V &= \frac{1}{a} + \sqrt{\frac{1}{a^2} + \xi_m^2} \operatorname{Re} \left[iK(m) - E(1-m) - iE(m) \right], \\ &= \frac{1}{a} + \sqrt{\frac{1}{a^2} + \xi_m^2} \operatorname{Re} \left[iK(m) - \tilde{E}(m) \right], \end{aligned} \quad (\text{A.14})$$

where we also explicitly used only a real part of the expression as it was done for L in (A.5) and defined common shorthand notation

$$\tilde{E}(m) = E(1 - m) + i E(m). \quad (\text{A.15})$$

Similarly, starting from (41), one can obtain the second form of the potential:

$$\pi\alpha'V = \frac{1}{a} - \frac{\mathcal{C}L}{2} + \frac{\xi_m\mathcal{C}}{n} \operatorname{Re} \left[\tilde{K}(m) - n\tilde{\Pi}(n, m) - \tilde{E}(m) \right], \quad (\text{A.16})$$

where

$$\tilde{K}(m) = mK(1 - m) + iK(m). \quad (\text{A.17})$$

ACKNOWLEDGMENTS

We are grateful to V. Braguta and E. Kolomeitsev for the valuable discussions. The work was supported by the grant BASIS #25-1-5-80-1.

[1] D. N. Voskresensky and N. Yu. Anisimov. Properties of a pion condensate in a magnetic field. *Zh. Eksp. Teor. Fiz.*, 78:2845–2853, 1980. [Sov. Phys. JETP **51**, 13 (1980)].

[2] V. Skokov, A. Y. Illarionov, and V. D. Toneev. Estimate of the magnetic field strength in heavy-ion collisions. *International Journal of Modern Physics A*, 24:5925–5932, 2009.

[3] Adam Bzdak and Vladimir Skokov. Event-by-event fluctuations of magnetic and electric fields in heavy ion collisions. *Phys. Lett. B*, 710:171–174, 2012.

[4] Wei-Tian Deng and Xu-Guang Huang. Event-by-event generation of electromagnetic fields in heavy-ion collisions. *Phys. Rev. C*, 85:044907, 2012.

[5] John Bloczynski, Xu-Guang Huang, Xilin Zhang, and Jinfeng Liao. Azimuthally fluctuating magnetic field and its impacts on observables in heavy-ion collisions. *Phys. Lett. B*, 718:1529–1535, 2013.

[6] Umut Gürsoy, Dmitri Kharzeev, and Krishna Rajagopal. Magnetohydrodynamics, charged currents and directed flow in heavy ion collisions. *Phys. Rev. C*, 89(5):054905, 2014.

[7] Gabriele Inghirami, Luca Del Zanna, Andrea Beraudo, Mohsen Haddadi Moghaddam, Francesco Becattini, and Marcus Bleicher. Numerical magneto-hydrodynamics for relativistic nuclear collisions. *Eur. Phys. J. C*, 76(12):659, 2016.

[8] V. Toneev, O. Rogachevsky, and V. Voronyuk. Evidence for creation of strong electromagnetic fields in relativistic heavy-ion collisions. *Eur. Phys. J. A*, 52(8):264, 2016.

[9] Umut Gürsoy, Dmitri Kharzeev, Eric Marcus, Krishna Rajagopal, and Chun Shen. Charge-dependent Flow Induced by Magnetic and Electric Fields in Heavy Ion Collisions. *Phys. Rev. C*, 98(5):055201, 2018.

[10] Bogdan V. Galilo and Sergei N. Nedelko. Impact of the strong electromagnetic field on the QCD effective potential for homogeneous Abelian gluon field configurations. *Phys. Rev. D*, 84:094017, 2011.

[11] G. S. Bali, F. Bruckmann, G. Endrodi, Z. Fodor, S. D. Katz, and A. Schafer. QCD quark condensate in external magnetic fields. *Phys. Rev. D*, 86:071502, 2012.

[12] Alejandro Ayala, M. Loewe, Ana Julia Mizher, and R. Zamora. Inverse magnetic catalysis for the chiral transition induced by thermo-magnetic effects on the coupling constant. *Phys. Rev. D*, 90(3):036001, 2014.

[13] Niklas Mueller and Jan M. Pawłowski. Magnetic catalysis and inverse magnetic catalysis in QCD. *Phys. Rev. D*, 91(11):116010, 2015.

[14] Shijun Mao. Inverse magnetic catalysis in Nambu–Jona-Lasinio model beyond mean field. *Phys. Lett. B*, 758:195–199, 2016.

[15] R. L. S. Farias, V. S. Timoteo, S. S. Avancini, M. B. Pinto, and G. Krein. Thermo-magnetic effects in quark matter: Nambu–Jona-Lasinio model constrained by lattice QCD. *Eur. Phys. J. A*, 53(5):101, 2017.

[16] V. V. Braguta, M. N. Chernodub, A. Yu Kotov, A. V. Molochkov, and A. A. Nikolaev. Finite-density QCD transition in a magnetic background field. *Phys. Rev. D*, 100(11):114503, 2019.

[17] Kenji Fukushima, Dmitri E. Kharzeev, and Harmen J. Warringa. The Chiral Magnetic Effect. *Phys. Rev. D*, 78:074033, 2008.

[18] A. V. Sadofyev, V. I. Shevchenko, and V. I. Zakharov. Notes on chiral hydrodynamics within effective theory approach. *Phys. Rev. D*, 83:105025, 2011.

[19] V. D. Toneev, V. P. Konchakovski, V. Voronyuk, E. L. Bratkovskaya, and W. Cassing. Event-by-event background in estimates of the chiral magnetic effect. *Phys. Rev. C*, 86:064907, 2012.

[20] Dmitri E. Kharzeev. The Chiral Magnetic Effect and Anomaly-Induced Transport. *Prog. Part. Nucl. Phys.*, 75:133–151, 2014.

[21] Francesco Becattini, Iurii Karpenko, Michael Annan Lisa, Isaac Upsal, and Sergei A. Voloshin. Global hyperon polarization at local thermodynamic equilibrium with vorticity, magnetic field, and feed-down. *Phys. Rev. C*, 95:054902, 2017.

[22] Yu Guo, Shuzhe Shi, Shengqin Feng, and Jinfeng Liao. Magnetic Field Induced Polarization Difference between Hyperons and Anti-hyperons. *Phys. Lett. B*, 798:134929, 2019.

[23] Yu-Chen Liu and Xu-Guang Huang. Spin polarization formula for Dirac fermions at local equilibrium. *Sci. China Phys. Mech. Astron.*, 65(7):272011, 2022.

[24] Kun Xu, Fan Lin, Anping Huang, and Mei Huang. Λ/Λ^- polarization and splitting induced by rotation and magnetic field. *Phys. Rev. D*, 106(7):L071502, 2022.

[25] Matteo Buzzegoli. Spin polarization induced by magnetic field and the relativistic Barnett effect. *Nucl. Phys. A*, 1036:122674, 2023.

[26] Zhiwei Liu, Yunfan Bai, Shiqi Zheng, Anping Huang, and Baoyi Chen. Exploring spin polarization of heavy quarks in magnetic fields and hot medium. *Phys. Rev. C*, 110(3):034910, 2024.

[27] Hideyoshi Taya, Toru Nishimura, and Akira Ohnishi. Estimation of electric field in intermediate-energy heavy-ion collisions. *Phys. Rev. C*, 110(1):014901, 2024.

[28] Julian S. Schwinger. On gauge invariance and vacuum polarization. *Phys. Rev.*, 82:664–679, 1951.

[29] Gerhard Baur, Kai Hencken, and Dirk Trautmann. Electron-Positron Pair Production in Relativistic Heavy Ion Collisions. *Phys. Rept.*, 453:1–27, 2007.

[30] Francois Gelis and Naoto Tanji. Schwinger mechanism revisited. *Prog. Part. Nucl. Phys.*, 87:1–49, 2016.

[31] B. I. Abelev et al. Global polarization measurement in Au+Au collisions. *Phys. Rev. C*, 76:024915, 2007. [Erratum: Phys.Rev.C 95, 039906 (2017)].

[32] L. Adamczyk et al. Global Λ hyperon polarization in nuclear collisions: evidence for the most vortical fluid. *Nature*, 548:62–65, 2017.

[33] J. Adam et al. Global Polarization of Ξ and Ω Hyperons in Au+Au Collisions at $\sqrt{s_{NN}} = 200$ GeV. *Phys. Rev. Lett.*, 126(16):162301, 2021. [Erratum: Phys.Rev.Lett. 131, 089901 (2023)].

[34] R. Abou Yassine et al. Measurement of global polarization of Λ hyperons in few-GeV heavy-ion collisions. *Phys. Lett. B*, 835:137506, 2022.

[35] Apostolos D. Panagiotou. Λ^0 nonpolarization: Possible signature of quark matter. *Phys. Rev. C*, 33:1999–2002, 1986.

[36] J. W. Harris, A. Sandoval, R. Stock, H. Stroebele, R. E. Renfordt, J. V. Geaga, H. G. Pugh, L. S. Schroeder, K. L. Wolf, and A. Dacal. Λ production near threshold in central nucleus-nucleus collisions. *Phys. Rev. Lett.*, 47:229–232, 1981.

[37] M. Anikina et al. Characteristics of λ and k^0 particles produced in central nucleus-nucleus collisions at a 4.5 gev/c momentum per incident nucleon. *Z. Phys. C*, 25:1–11, 1984.

[38] Jian-Hua Gao, Zuo-Tang Liang, Shi Pu, Qun Wang, and Xin-Nian Wang. Chiral anomaly and local polarization effect from the quantum kinetic approach. *Phys. Rev. Lett.*, 109:232301, 2012.

[39] F. Becattini, V. Chandra, L. Del Zanna, and E. Grossi. Relativistic distribution function for particles with spin at local thermodynamical equilibrium. *Annals Phys.*, 338:32–49, 2013.

[40] Alexander Sorin and Oleg Teryaev. Axial anomaly and energy dependence of hyperon polarization in Heavy-Ion Collisions. *Phys. Rev. C*, 95(1):011902, 2017.

[41] Oleg V. Teryaev and Valentin I. Zakharov. From the chiral vortical effect to polarization of baryons: A model. *Phys. Rev. D*, 96(9):096023, 2017.

[42] L. P. Csernai, J. I. Kapusta, and T. Welle. Λ and $\bar{\Lambda}$ spin interaction with meson fields generated by the baryon current in high energy nuclear collisions. *Phys. Rev. C*, 99(2):021901, 2019.

[43] F. Becattini, M. Buzzegoli, and A. Palermo. Spin-thermal shear coupling in a relativistic fluid. *Physics Letters B*, 820:136519, 2021.

[44] Shuai Y. F. Liu and Yi Yin. Spin polarization induced by the hydrodynamic gradients. *JHEP*, 07:188, 2021.

[45] Cong Yi, Shi Pu, and Di-Lun Yang. Reexamination of local spin polarization beyond global equilibrium in relativistic heavy ion collisions. *Phys. Rev. C*, 104(6):064901, 2021.

[46] Shuai Y. F. Liu and Yi Yin. Spin hall effect in heavy-ion collisions. *Phys. Rev. D*, 104:054043, 2021.

[47] Shu Lin and Ziyue Wang. Shear induced polarization: collisional contributions. *JHEP*, 12:030, 2022.

[48] F. Becattini, L. Csernai, and D. J. Wang. Λ polarization in peripheral heavy ion collisions. *Phys. Rev. C*, 88(3):034905, 2013. [Erratum: Phys.Rev.C 93, 069901 (2016)].

[49] F. Becattini, G. Inghirami, V. Rolando, A. Beraudo, L. Del Zanna, A. De Pace, M. Nardi, G. Pagliara, and V. Chandra. A study of vorticity formation in high energy nuclear collisions. *Eur. Phys. J. C*, 75(9):406, 2015. [Erratum: Eur.Phys.J.C 78, 354 (2018)].

[50] F. Becattini, F. Piccinini, and J. Rizzo. Angular momentum conservation in heavy ion collisions at very high energy. *Phys. Rev. C*, 77:024906, 2008.

[51] Jian-Hua Gao, Shou-Wan Chen, Wei-Tian Deng, Zuo-Tang Liang, Qun Wang, and Xin-Nian Wang. Global quark polarization in non-central A+A collisions. *Phys. Rev. C*, 77:044902, 2008.

[52] Yin Jiang, Zi-Wei Lin, and Jinfeng Liao. Rotating quark-gluon plasma in relativistic heavy ion collisions. *Phys. Rev. C*, 94(4):044910, 2016. [Erratum: Phys.Rev.C 95, 049904 (2017)].

[53] Nils Sass, Marco Müller, Oscar Garcia-Montero, and Hannah Elfner. Global angular momentum generation in heavy-ion reactions within a hadronic transport approach. *Phys. Rev. C*, 108(4):044903, 2023.

[54] N. S. Tsegelnik, E. E. Kolomeitsev, and V. Voronyuk. Helicity and vorticity in heavy-ion collisions at energies available at the JINR Nuclotron-based Ion Collider facility. *Phys. Rev. C*, 107(3):034906, 2023.

[55] Oleg Teryaev and Rahim Usubov. Vorticity and hydrodynamic helicity in heavy-ion collisions in the hadron-string

dynamics model. *Phys. Rev. C*, 92(1):014906, 2015.

[56] Mircea Baznat, Konstantin Gudima, Alexander Sorin, and Oleg Teryaev. Femto-vortex sheets and hyperon polarization in heavy-ion collisions. *Phys. Rev. C*, 93:031902, 2016.

[57] Wei-Tian Deng and Xu-Guang Huang. Vorticity in heavy-ion collisions. *Phys. Rev. C*, 93:064907, 2016.

[58] Yu. B. Ivanov and A. A. Soldatov. Vorticity in heavy-ion collisions at the JINR Nuclotron-based Ion Collider fAcility. *Phys. Rev. C*, 95(5):054915, 2017.

[59] Xiao-Liang Xia, Hui Li, Ze-Bo Tang, and Qun Wang. Probing vorticity structure in heavy-ion collisions by local Λ polarization. *Phys. Rev. C*, 98:024905, 2018.

[60] E. E. Kolomeitsev, V. D. Toneev, and V. Voronyuk. Vorticity and hyperon polarization at energies available at JINR Nuclotron-based Ion Collider fAcility. *Phys. Rev. C*, 97(6):064902, 2018.

[61] Xian-Gai Deng, Xu-Guang Huang, Yu-Gang Ma, and Song Zhang. Vorticity in low-energy heavy-ion collisions. *Phys. Rev. C*, 101:064908, 2020.

[62] H. Petersen. The fastest-rotating fluid. *Nature*, 548:34–35, 2017.

[63] G. Yu. Prokhorov, D. A. Shohonov, O. V. Teryaev, N. S. Tsegelnik, and V. I. Zakharov. Modeling of acceleration in heavy-ion collisions: Occurrence of temperature below the Unruh temperature. *Phys. Rev. C*, 112(6):064907, 2025.

[64] W. G. Unruh. Second quantization in the Kerr metric. *Phys. Rev. D*, 10:3194–3205, 1974.

[65] A. Vilenkin. Macroscopic parity violating effects: neutrino fluxes from rotating black holes and in rotating thermal radiation. *Phys. Rev. D*, 20:1807–1812, 1979.

[66] John R. Letaw and Jonathan D. Pfautsch. The Quantized Scalar Field in Rotating Coordinates. *Phys. Rev. D*, 22:1345, 1980.

[67] Bala R. Iyer. Dirac field theory in rotating coordinates. *Phys. Rev. D*, 26:1900–1905, 1982.

[68] Paul C. W. Davies, Tevian Dray, and Corinne A. Manogue. The Rotating quantum vacuum. *Phys. Rev. D*, 53:4382–4387, 1996.

[69] Gavin Duffy and Adrian C. Ottewill. The Rotating quantum thermal distribution. *Phys. Rev. D*, 67:044002, 2003.

[70] Uwe R. Fischer and Gordon Baym. Vortex states of rapidly rotating dilute Bose-Einstein condensates. *Phys. Rev. Lett.*, 90:140402, 2003.

[71] Arata Yamamoto and Yuji Hirono. Lattice QCD in rotating frames. *Phys. Rev. Lett.*, 111:081601, 2013.

[72] Victor E. Ambruš and Elizabeth Winstanley. Rotating quantum states. *Phys. Lett. B*, 734:296–301, 2014.

[73] Shu Ebihara, Kenji Fukushima, and Kazuya Mameda. Boundary effects and gapped dispersion in rotating fermionic matter. *Phys. Lett. B*, 764:94–99, 2017.

[74] Yin Jiang and Jinfeng Liao. Pairing Phase Transitions of Matter under Rotation. *Phys. Rev. Lett.*, 117(19):192302, 2016.

[75] M. N. Chernodub and Shinya Gongyo. Interacting fermions in rotation: chiral symmetry restoration, moment of inertia and thermodynamics. *JHEP*, 01:136, 2017.

[76] Xinyang Wang, Minghua Wei, Zhibin Li, and Mei Huang. Quark matter under rotation in the NJL model with vector interaction. *Phys. Rev. D*, 99(1):016018, 2019.

[77] Hui Zhang, Defu Hou, and Jinfeng Liao. Mesonic Condensation in Isospin Matter under Rotation. *Chin. Phys. C*, 44(11):111001, 2020.

[78] M. N. Chernodub. Inhomogeneous confining-deconfining phases in rotating plasmas. *Phys. Rev. D*, 103(5):054027, 2021.

[79] Yuki Fujimoto, Kenji Fukushima, and Yoshimasa Hidaka. Deconfining Phase Boundary of Rapidly Rotating Hot and Dense Matter and Analysis of Moment of Inertia. *Phys. Lett. B*, 816:136184, 2021.

[80] Shi Chen, Kenji Fukushima, and Yusuke Shimada. Perturbative Confinement in Thermal Yang-Mills Theories Induced by Imaginary Angular Velocity. *Phys. Rev. Lett.*, 129(24):242002, 2022.

[81] Hao-Lei Chen, Zhi-Bin Zhu, and Xu-Guang Huang. Quark-meson model under rotation: A functional renormalization group study. *Phys. Rev. D*, 108(5):054006, 2023.

[82] Fei Sun, Kun Xu, and Mei Huang. Splitting of chiral and deconfinement phase transitions induced by rotation. *Phys. Rev. D*, 108(9):096007, 2023.

[83] Victor E. Ambruš and Maxim N. Chernodub. Rigidly rotating scalar fields: Between real divergence and imaginary fractalization. *Phys. Rev. D*, 108(8):085016, 2023.

[84] D. N. Voskresensky. Pion-sigma meson vortices in rotating systems. *Phys. Rev. D*, 109(3):034030, 2024.

[85] Fei Sun, Jingdong Shao, Rui Wen, Kun Xu, and Mei Huang. Chiral phase transition and spin alignment of vector mesons in the polarized-Polyakov-loop Nambu–Jona-Lasinio model under rotation. *Phys. Rev. D*, 109(11):116017, 2024.

[86] Maxim Chernodub. Negative moment of inertia of large- N_c gluons on a ring. 6 2025.

[87] Lutz Kiefer, Ashutosh Dash, and Dirk H. Rischke. Magnetization by Rotation: Spin and Chiral Condensates in the NJL Model. 9 2025.

[88] William G. Unruh and Nathan Weiss. Acceleration Radiation in Interacting Field Theories. *Phys. Rev. D*, 29:1656, 1984.

[89] Tadafumi Ohsaku. Dynamical chiral symmetry breaking and its restoration for an accelerated observer. *Phys. Lett. B*, 599:102–110, 2004.

[90] Jan Ivar Korsbakken and Jon Magne Leinaas. The Fulling-Unruh effect in general stationary accelerated frames. *Phys. Rev. D*, 70:084016, 2004.

[91] D. Ebert and V. Ch. Zhukovsky. Restoration of Dynamically Broken Chiral and Color Symmetries for an Accelerated Observer. *Phys. Lett. B*, 645:267–274, 2007.

[92] P. Castorina and M. Finocchiaro. Symmetry Restoration By Acceleration. *J. Mod. Phys.*, 3:1703, 2012.

[93] Shingo Takeuchi. Bose–Einstein condensation in the Rindler space. *Phys. Lett. B*, 750:209–217, 2015.

[94] Sanjin Benic and Kenji Fukushima. Unruh effect and condensate in and out of an accelerated vacuum. 2015.

[95] F. Becattini. Thermodynamic equilibrium with acceleration and the Unruh effect. *Phys. Rev. D*, 97(8):085013, 2018.

[96] George Y. Prokhorov, Oleg V. Teryaev, and Valentin I. Zakharov. Effects of rotation and acceleration in the axial current: density operator vs Wigner function. *JHEP*, 02:146, 2019.

[97] G. Prokhorov, O. Teryaev, and V. Zakharov. Axial current in rotating and accelerating medium. *Phys. Rev. D*, 98(7):071901, 2018.

[98] Fabio Scardigli, Massimo Blasone, Gaetano Luciano, and Roberto Casadio. Modified Unruh effect from Generalized Uncertainty Principle. *Eur. Phys. J. C*, 78(9):728, 2018.

[99] George Y. Prokhorov, Oleg V. Teryaev, and Valentin I. Zakharov. Unruh effect for fermions from the Zubarev density operator. *Phys. Rev. D*, 99(7):071901, 2019.

[100] Andrea Palermo, Matteo Buzzegoli, and Francesco Becattini. Exact equilibrium distributions in statistical quantum field theory with rotation and acceleration: Dirac field. *JHEP*, 10:077, 2021.

[101] E. T. Akhmedov, K. V. Bazarov, and D. V. Diakonov. Quantum fields in the future Rindler wedge. *Phys. Rev. D*, 104(8):085008, 2021.

[102] M. N. Chernodub, V. A. Goy, A. V. Molochkov, D. V. Stepanov, and A. S. Pochinok. Extreme Softening of QCD Phase Transition under Weak Acceleration: First-Principles Monte Carlo Results for Gluon Plasma. *Phys. Rev. Lett.*, 134(11):111904, 2025.

[103] Maxim N. Chernodub. Acceleration as refrigeration: Acceleration-induced spontaneous symmetry breaking in thermal medium. 2025.

[104] M. Bordag and D. N. Voskresensky. Charged scalar bosons under rotation and acceleration. 10 2025.

[105] G. Yu. Prokhorov. Entanglement Viscosity: from Unitarity to Irreversibility in Accelerated Frames. 1 2026.

[106] Hao-Lei Chen, Kenji Fukushima, Xu-Guang Huang, and Kazuya Mameda. Analogy between rotation and density for Dirac fermions in a magnetic field. *Phys. Rev. D*, 93(10):104052, 2016.

[107] Yizhuang Liu and Ismail Zahed. Pion Condensation by Rotation in a Magnetic field. *Phys. Rev. Lett.*, 120(3):032001, 2018.

[108] Yizhuang Liu and Ismail Zahed. Rotating Dirac fermions in a magnetic field in 1+2 and 1+3 dimensions. *Phys. Rev. D*, 98(1):014017, 2018.

[109] Kenji Fukushima. Extreme matter in electromagnetic fields and rotation. *Prog. Part. Nucl. Phys.*, 107:167–199, 2019.

[110] N. Sadooghi, S. M. A. Tabatabaei Mehr, and F. Taghinavaz. Inverse magnetorotational catalysis and the phase diagram of a rotating hot and magnetized quark matter. *Phys. Rev. D*, 104(11):116022, 2021.

[111] D. N. Voskresensky. Pion condensation at rotation in magnetic field, electric, and scalar potential wells. *Phys. Rev. D*, 111(3):036022, 2025.

[112] V. V. Braguta, A. Yu. Kotov, D. D. Kuznedelev, and A. A. Roenko. Study of the Confinement/Deconfinement Phase Transition in Rotating Lattice SU(3) Gluodynamics. *Pisma Zh. Eksp. Teor. Fiz.*, 112(1):9–16, 2020.

[113] V. V. Braguta, A. Yu. Kotov, D. D. Kuznedelev, and A. A. Roenko. Influence of relativistic rotation on the confinement-deconfinement transition in gluodynamics. *Phys. Rev. D*, 103(9):094515, 2021.

[114] Victor Braguta, A. Yu. Kotov, Denis Kuznedelev, and Artem Roenko. Lattice study of the confinement/deconfinement transition in rotating gluodynamics. *PoS*, LATTICE2021:125, 2022.

[115] V. V. Braguta, Andrey Kotov, Artem Roenko, and Dmitry Sychev. Thermal phase transitions in rotating QCD with dynamical quarks. *PoS*, LATTICE2022:190, 2023.

[116] V. V. Braguta, M. N. Chernodub, I. E. Kudrov, A. A. Roenko, and D. A. Sychev. Influence of Relativistic Rotation on QCD Properties. *Phys. Atom. Nucl.*, 86(6):1249–1255, 2023.

[117] Ji-Chong Yang and Xu-Guang Huang. QCD on Rotating Lattice with Staggered Fermions. 2023.

[118] M. N. Chernodub, V. A. Goy, and A. V. Molochkov. Inhomogeneity of a rotating gluon plasma and the Tolman-Ehrenfest law in imaginary time: Lattice results for fast imaginary rotation. *Phys. Rev. D*, 107(11):114502, 2023.

[119] V. V. Braguta, I. E. Kudrov, A. A. Roenko, D. A. Sychev, and M. N. Chernodub. Lattice Study of the Equation of State of a Rotating Gluon Plasma. *JETP Lett.*, 117(9):639–644, 2023.

[120] Victor V. Braguta, Maxim N. Chernodub, Artem A. Roenko, and Dmitrii A. Sychev. Negative moment of inertia and rotational instability of gluon plasma. *Phys. Lett. B*, 852:138604, 2024.

[121] Victor V. Braguta, Maxim N. Chernodub, Ilya E. Kudrov, Artem A. Roenko, and Dmitrii A. Sychev. Moment of inertia and supervortical temperature of gluon plasma. *PoS*, LATTICE2023:181, 2024.

[122] Victor V. Braguta, Maxim N. Chernodub, Ilya E. Kudrov, Artem A. Roenko, and Dmitrii A. Sychev. Negative Barnett effect, negative moment of inertia of the gluon plasma, and thermal evaporation of the chromomagnetic condensate. *Phys. Rev. D*, 110(1):014511, 2024.

[123] Victor V. Braguta, Maxim N. Chernodub, and Artem A. Roenko. New mixed inhomogeneous phase in vortical gluon plasma: First-principle results from rotating SU(3) lattice gauge theory. *Phys. Lett. B*, 855:138783, 2024.

[124] V. Braguta, M. Chernodub, E. Eremeev, I. Kudrov, A. Roenko, and D. Sychev. On the angular momentum and free energy of rotating gluon plasma. 12 2025.

[125] Juan Martin Maldacena. The Large N limit of superconformal field theories and supergravity. *Adv. Theor. Math. Phys.*, 2:231–252, 1998.

[126] Oliver DeWolfe, Steven S. Gubser, Christopher Rosen, and Derek Teaney. Heavy ions and string theory. *Prog. Part. Nucl. Phys.*, 75:86–132, 2014.

[127] Jorge Casalderrey-Solana, Hong Liu, David Mateos, Krishna Rajagopal, and Urs Achim Wiedemann. *Gauge/String Duality, Hot QCD and Heavy Ion Collisions*. Cambridge University Press, 2014.

[128] I. Ya Aref'eva. Holographic approach to quark-gluon plasma in heavy ion collisions. *Phys. Usp.*, 57:527–555, 2014.

- [129] Juan Maldacena. Wilson loops in large N field theories. *Phys. Rev. Lett.*, 80:4859–4862, Jun 1998.
- [130] Soo-Jong Rey, Stefan Theisen, and Jung-Tay Yee. Wilson-polyakov loop at finite temperature in large- n gauge theory and anti-de sitter supergravity. *Nuclear Physics B*, 527(1):171–186, 1998.
- [131] A Brandhuber, N Itzhaki, J Sonnenschein, and S Yankielowicz. Wilson loops in the large n limit at finite temperature. *Physics Letters B*, 434(1):36–40, 1998.
- [132] A. Brandhuber and K. Sfetsos. Wilson loops from multicenter and rotating branes, mass gaps and phase structure in gauge theories. *Adv. Theor. Math. Phys.*, 3:851–887, 1999.
- [133] Y. Kinar, E. Schreiber, and J. Sonnenschein. $q\bar{Q}$ potential from strings in curved space-time – classical results. *Nuclear Physics B*, 566(1):103–125, 2000.
- [134] Soo-Jong Rey and Jung-Tay Yee. Macroscopic strings as heavy quarks in large N gauge theory and anti-de Sitter supergravity. *Eur. Phys. J. C*, 22:379–394, 2001.
- [135] Henrique Boschi-Filho, Nelson R. F. Braga, and Cristine N. Ferreira. Heavy quark potential at finite temperature from gauge/string duality. *Phys. Rev. D*, 74:086001, 2006.
- [136] Hong Liu, Krishna Rajagopal, and Urs Achim Wiedemann. Wilson loops in heavy ion collisions and their calculation in AdS/CFT. *JHEP*, 03:066, 2007.
- [137] C D White. The Cornell potential from general geometries in AdS / QCD. *Phys. Lett. B*, 652:79–85, 2007.
- [138] Dimitrios Giataganas. Probing strongly coupled anisotropic plasma. *Journal of High Energy Physics*, 2012(7):31, 2012.
- [139] Dimitrios Giataganas and Nikos Irges. Flavor Corrections in the Static Potential in Holographic QCD. *Phys. Rev. D*, 85:046001, 2012.
- [140] Edward Witten. Anti-de Sitter space, thermal phase transition, and confinement in gauge theories. *Adv. Theor. Math. Phys.*, 2:505–532, 1998.
- [141] Bo Sundborg. The hagedorn transition, deconfinement and $n=4$ sym theory. *Nuclear Physics B*, 573(1):349–363, 2000.
- [142] Marcus Spradlin and Anastasia Volovich. The one-loop partition function of $n=4$ super-yang–mills theory on $\mathbb{R} \times s^3$. *Nuclear Physics B*, 711(1):199–230, 2005.
- [143] Joseph Polchinski and Matthew J. Strassler. The String dual of a confining four-dimensional gauge theory. 3 2000.
- [144] Y. M. Cho and Ishwaree P. Neupane. Anti-de Sitter black holes, thermal phase transition and holography in higher curvature gravity. *Phys. Rev. D*, 66:024044, 2002.
- [145] Ofer Aharony, Joseph Marsano, Shiraz Minwalla, Kyriakos Papadodimas, and Mark Van Raamsdonk. The Hagedorn - deconfinement phase transition in weakly coupled large N gauge theories. *Adv. Theor. Math. Phys.*, 8:603–696, 2004.
- [146] Andreas Karch, Emanuel Katz, Dam T. Son, and Mikhail A. Stephanov. Linear confinement and AdS/QCD. *Phys. Rev. D*, 74:015005, 2006.
- [147] C. A. Ballon Bayona, Henrique Boschi-Filho, Nelson R. F. Braga, and Leopoldo A. Pando Zayas. On a Holographic Model for Confinement/Deconfinement. *Phys. Rev. D*, 77:046002, 2008.
- [148] U. Gursoy, E. Kiritsis, L. Mazzanti, and F. Nitti. Holography and Thermodynamics of 5D Dilaton-gravity. *JHEP*, 05:033, 2009.
- [149] Donald Marolf, Mukund Rangamani, and Toby Wiseman. Holographic thermal field theory on curved spacetimes. *Class. Quant. Grav.*, 31:063001, 2014.
- [150] Stanley J. Brodsky, Guy F. de Teramond, Hans Gunter Dosch, and Joshua Erlich. Light-Front Holographic QCD and Emerging Confinement. *Phys. Rept.*, 584:1–105, 2015.
- [151] Troels Harmark and Matthias Wilhelm. Hagedorn temperature of $\text{ads}_5/\text{cft}_4$ via integrability. *Phys. Rev. Lett.*, 120:071605, Feb 2018.
- [152] Sang-Jin Sin and Ismail Zahed. Holography of radiation and jet quenching. *Phys. Lett. B*, 608:265–273, 2005.
- [153] Christopher P. Herzog. Energy Loss of Heavy Quarks from Asymptotically AdS Geometries. *JHEP*, 09:032, 2006.
- [154] C. P. Herzog, A. Karch, P. Kovtun, C. Kozcaz, and L. G. Yaffe. Energy loss of a heavy quark moving through $N=4$ supersymmetric Yang-Mills plasma. *JHEP*, 07:013, 2006.
- [155] Steven S. Gubser. Drag force in AdS/CFT. *Phys. Rev. D*, 74:126005, 2006.
- [156] Hong Liu, Krishna Rajagopal, and Urs Achim Wiedemann. Calculating the jet quenching parameter from AdS/CFT. *Phys. Rev. Lett.*, 97:182301, 2006.
- [157] Mariano Chernicoff, Daniel Fernandez, David Mateos, and Diego Trancanelli. Jet quenching in a strongly coupled anisotropic plasma. *JHEP*, 08:041, 2012.
- [158] Emil T. Akhmedov. A Remark on the AdS / CFT correspondence and the renormalization group flow. *Phys. Lett. B*, 442:152–158, 1998.
- [159] Dam T. Son and Andrei O. Starinets. Minkowski space correlators in AdS / CFT correspondence: Recipe and applications. *JHEP*, 09:042, 2002.
- [160] Joseph Polchinski and Matthew J. Strassler. Hard scattering and gauge / string duality. *Phys. Rev. Lett.*, 88:031601, 2002.
- [161] Henrique Boschi-Filho and Nelson R. F. Braga. Gauge / string duality and scalar glueball mass ratios. *JHEP*, 05:009, 2003.
- [162] Henrique Boschi-Filho and Nelson R. F. Braga. QCD / string holographic mapping and glueball mass spectrum. *Eur. Phys. J. C*, 32:529–533, 2004.
- [163] P. Kovtun, Dan T. Son, and Andrei O. Starinets. Viscosity in strongly interacting quantum field theories from black hole physics. *Phys. Rev. Lett.*, 94:111601, 2005.
- [164] Jorge Casalderrey-Solana and Derek Teaney. Heavy quark diffusion in strongly coupled $N=4$ Yang-Mills. *Phys. Rev. D*, 74:085012, 2006.

[165] Hong Liu, Krishna Rajagopal, and Urs Achim Wiedemann. An AdS/CFT Calculation of Screening in a Hot Wind. *Phys. Rev. Lett.*, 98:182301, 2007.

[166] Shinsei Ryu and Tadashi Takayanagi. Holographic derivation of entanglement entropy from AdS/CFT. *Phys. Rev. Lett.*, 96:181602, 2006.

[167] Edward Shuryak, Sang-Jin Sin, and Ismail Zahed. A Gravity dual of RHIC collisions. *J. Korean Phys. Soc.*, 50:384–397, 2007.

[168] Daniel Grumiller and Paul Romatschke. On the collision of two shock waves in AdS(5). *JHEP*, 08:027, 2008.

[169] N. P. Bobev, H. Dimov, and R. C. Rashkov. Semiclassical strings in Lunin-Maldacena background. *Bulg. J. Phys.*, 35:274–285, 2008.

[170] Steven S. Gubser, Silviu S. Pufu, and Amos Yarom. Off-center collisions in AdS(5) with applications to multiplicity estimates in heavy-ion collisions. *JHEP*, 11:050, 2009.

[171] E. T. Akhmedov, I. B. Gahramanov, and E. T. Musaev. Hints on integrability in the Wilsonian/holographic renormalization group. *JETP Lett.*, 93:545–550, 2011.

[172] David Mateos and Diego Trancanelli. The anisotropic N=4 super Yang-Mills plasma and its instabilities. *Phys. Rev. Lett.*, 107:101601, 2011.

[173] Michael Strickland. Thermalization and isotropization in heavy-ion collisions. *Pramana*, 84(5):671–684, 2015.

[174] Dimitrios Giataganas, Umut Gürsoy, and Juan F. Pedraza. Strongly-coupled anisotropic gauge theories and holography. *Phys. Rev. Lett.*, 121(12):121601, 2018.

[175] Chong-Sun Chu and Dimitrios Giataganas. c -Theorem for Anisotropic RG Flows from Holographic Entanglement Entropy. *Phys. Rev. D*, 101(4):046007, 2020.

[176] H. Dimov, R. C. Rashkov, and T. Vetsov. Thermodynamic information geometry and complexity growth of a warped AdS black hole and the warped AdS₃/CFT₂ correspondence. *Phys. Rev. D*, 99(12):126007, 2019.

[177] Dimitrios Giataganas. Velocity Laws for Bound States in Asymptotically AdS Geometries. *Fortsch. Phys.*, 71(4–5):2300030, 2023.

[178] V. Avramov, H. Dimov, M. Radomirov, R. C. Rashkov, and T. Vetsov. On thermodynamic stability of black holes. Part I: classical stability. *Eur. Phys. J. C*, 84(3):281, 2024.

[179] Ksenia Arkhipova, Lev Astrakhantsev, Nihat Sadik Deger, Anastasia A. Golubtsova, Kirill Gubarev, and Edvard T. Musaev. Holographic RG flows and boundary conditions in a 3D gauged supergravity. *Eur. Phys. J. C*, 84(6):560, 2024.

[180] Lev Astrakhantsev, Anastasia A. Golubtsova, and Mikhail A. Podoinitsyn. Zoo of flows in a 3d gauged supergravity with periodic potential. 11 2025.

[181] S. W. Hawking and H. S. Reall. Charged and rotating AdS black holes and their CFT duals. *Phys. Rev. D*, 61:024014, 2000.

[182] Elena Caceres and Alberto Guijosa. Drag force in charged N=4 SYM plasma. *JHEP*, 11:077, 2006.

[183] Eric D'Hoker and Per Kraus. Charged Magnetic Brane Solutions in AdS (5) and the fate of the third law of thermodynamics. *JHEP*, 03:095, 2010.

[184] Alfonso Ballon-Bayona. Holographic deconfinement transition in the presence of a magnetic field. *JHEP*, 11:168, 2013.

[185] David Dудal and Thomas G. Mertens. Melting of charmonium in a magnetic field from an effective AdS/QCD model. *Phys. Rev. D*, 91:086002, 2015.

[186] Nick Evans, Carlsson Miller, and Marc Scott. Inverse Magnetic Catalysis in Bottom-Up Holographic QCD. *Phys. Rev. D*, 94(7):074034, 2016.

[187] Danning Li, Mei Huang, Yi Yang, and Pei-Hung Yuan. Inverse Magnetic Catalysis in the Soft-Wall Model of AdS/QCD. *JHEP*, 02:030, 2017.

[188] Irina Aref'eva and Kristina Rannu. Holographic Anisotropic Background with Confinement-Deconfinement Phase Transition. *JHEP*, 05:206, 2018.

[189] Nelson R. F. Braga and Luiz F. Ferreira. Heavy meson dissociation in a plasma with magnetic fields. *Phys. Lett. B*, 783:186–192, 2018.

[190] David Dудal and Thomas G. Mertens. Holographic estimate of heavy quark diffusion in a magnetic field. *Phys. Rev. D*, 97(5):054035, 2018.

[191] Wenxing Cheng and Zi-qiang Zhang. Heavy quark potential in STU and AdS₅–Reissner–Nordstrom backgrounds. *Eur. Phys. J. C*, 85(7):774, 2025.

[192] S. W. Hawking, C. J. Hunter, and Marika Taylor. Rotation and the AdS / CFT correspondence. *Phys. Rev. D*, 59:064005, 1999.

[193] G. W. Gibbons, M. J. Perry, and C. N. Pope. The First law of thermodynamics for Kerr-anti-de Sitter black holes. *Class. Quant. Grav.*, 22:1503–1526, 2005.

[194] Sayantani Bhattacharyya, Subhaneil Lahiri, R. Loganayagam, and Shiraz Minwalla. Large rotating AdS black holes from fluid mechanics. *JHEP*, 09:054, 2008.

[195] A. Nata Atmaja and K. Schalm. Anisotropic Drag Force from 4D Kerr-AdS Black Holes. *JHEP*, 04:070, 2011.

[196] Brett McInnes. Applied holography of the AdS₅–Kerr space–time. *Int. J. Mod. Phys. A*, 34(24):1950138, 2019.

[197] Irina Ya. Aref'eva, Anastasia A. Golubtsova, and Eric Gourgoulhon. Holographic drag force in 5d Kerr-AdS black hole. *JHEP*, 04:169, 2021.

[198] Anastasia A. Golubtsova, Eric Gourgoulhon, and Marina K. Usova. Heavy quarks in rotating plasma via holography. *Nucl. Phys. B*, 979:115786, 2022.

[199] Nelson R. F. Braga, Luiz F. Faulhaber, and Octavio C. Junqueira. Confinement-deconfinement temperature for a rotating quark-gluon plasma. *Phys. Rev. D*, 105(10):106003, 2022.

[200] Yidian Chen, Danning Li, and Mei Huang. Inhomogeneous chiral condensation under rotation in the holographic QCD. *Phys. Rev. D*, 106(10):106002, 2022.

[201] Brett McInnes. Why is black hole entropy affected by rotation? *JHEP*, 02:072, 2023.

[202] Gopal Yadav. Deconfinement temperature of rotating QGP at intermediate coupling from M-theory. *Phys. Lett. B*, 841:137925, 2023.

[203] Nelson R. F. Braga, Luiz F. Ferreira, and Octavio C. Junqueira. Configuration entropy of a rotating quark-gluon plasma from holography. *Phys. Lett. B*, 847:138265, 2023.

[204] Nelson R. F. Braga and Yan F. Ferreira. Bottomonium dissociation in a rotating plasma. *Phys. Rev. D*, 108(9):094017, 2023.

[205] Anastasia Golubtsova and Nikita Tsegelnik. Probing the holographic model of $\mathcal{N} = 4$ sym rotating quark-gluon plasma. *Phys. Rev. D*, 107:106017, 2023.

[206] Jun-Xia Chen and De-Fu Hou. Heavy quark potential and jet quenching parameter in a rotating D-instanton background. *Eur. Phys. J. C*, 84(4):447, 2024.

[207] Jun-Xia Chen, De-Fu Hou, and Hai-Cang Ren. Drag force and heavy quark potential in a rotating background. *JHEP*, 03:171, 2024.

[208] Nelson R. F. Braga and Octavio C. Junqueira. Inhomogeneity of a rotating quark-gluon plasma from holography. *Phys. Lett. B*, 848:138330, 2024.

[209] Yi-ze Cai and Zi-qiang Zhang. Holographic Schwinger effect in spinning black hole backgrounds. *Chin. Phys. C*, 48(1):015102, 2024.

[210] Jun-Xia Chen, Sheng Wang, Defu Hou, and Hai-Cang Ren. String tension and Polyakov loop in a rotating background. *Phys. Rev. D*, 111(2):026020, 2025.

[211] Luiz F. Ferreira. Dispersion relations and pole-skipping in a holographic charmonium model with rotating plasma. *Phys. Rev. D*, 112(7):074043, 2025.

[212] Zhou-Run Zhu, Sheng Wang, Man-Li Tian, and Defu Hou. Running coupling constant and jet quenching parameter in the spinning background from holography. 12 2025.

[213] Nelson R. F. Braga and Octavio C. Junqueira. Holographic QCD phase diagram for a rotating plasma in the Hawking-Page approach. *Phys. Lett. B*, 868:139669, 2025.

[214] Brett McInnes. Angular Momentum in QGP Holography. *Nucl. Phys. B*, 887:246–264, 2014.

[215] Brett McInnes. A rotation/magnetism analogy for the quark-gluon plasma. *Nucl. Phys. B*, 911:173–190, 2016.

[216] Xun Chen, Lin Zhang, Danning Li, Defu Hou, and Mei Huang. Gluodynamics and deconfinement phase transition under rotation from holography. *JHEP*, 07:132, 2021.

[217] Defu Hou, Mahdi Atashi, Kazem Bitaghsir Fadafan, and Zi-qiang Zhang. Holographic energy loss of a rotating heavy quark at finite chemical potential. *Phys. Lett. B*, 817:136279, 2021.

[218] Luis A. H. Mamani, Defu Hou, and Nelson R. F. Braga. Melting of heavy vector mesons and quasinormal modes in a finite density plasma from holography. *Phys. Rev. D*, 105(12):126020, 2022.

[219] Yan-Qing Zhao, Song He, Defu Hou, Li Li, and Zhibin Li. Phase diagram of holographic thermal dense QCD matter with rotation. *JHEP*, 04:115, 2023.

[220] Jia-Hao Wang and Sheng-Qin Feng. Rotation effect on the deconfinement phase transition in holographic QCD. *Phys. Rev. D*, 109(6):066019, 2024.

[221] Yidian Chen, Xun Chen, Danning Li, and Mei Huang. Deconfinement and chiral restoration phase transition under rotation from holography in an anisotropic gravitational background. *Phys. Rev. D*, 111(4):046006, 2025.

[222] Hiwa A. Ahmed, Yidian Chen, and Mei Huang. Gluon polarization contribution to the spin alignment of vector mesons from holography. *Phys. Rev. D*, 111(8):086006, 2025.

[223] Stanley Deser and Orit Levin. Accelerated detectors and temperature in (anti)-de Sitter spaces. *Class. Quant. Grav.*, 14:L163–L168, 1997.

[224] Alex Hamilton, Daniel N. Kabat, Gilad Lifschytz, and David A. Lowe. Holographic representation of local bulk operators. *Phys. Rev. D*, 74:066009, 2006.

[225] J. Podolsky and J. B. Griffiths. Accelerating Kerr-Newman black holes in (anti)-de Sitter space-time. *Phys. Rev. D*, 73:044018, 2006.

[226] Mariano Chernicoff and Alberto Guijosa. Acceleration, Energy Loss and Screening in Strongly-Coupled Gauge Theories. *JHEP*, 06:005, 2008.

[227] J. G. Russo and P. K. Townsend. Accelerating Branes and Brane Temperature. *Class. Quant. Grav.*, 25:175017, 2008.

[228] Mariano Chernicoff and Angel Paredes. Accelerated detectors and worldsheet horizons in AdS/CFT. *JHEP*, 03:063, 2011.

[229] Bartłomiej Czech, Joanna L. Karczmarek, Fernando Nogueira, and Mark Van Raamsdonk. Rindler Quantum Gravity. *Class. Quant. Grav.*, 29:235025, 2012.

[230] Maulik Parikh, Prasant Samantray, and Erik Verlinde. Rotating Rindler-AdS Space. *Phys. Rev. D*, 86:024005, 2012.

[231] Reza Fareghbal and Ali Naseh. Rindler/Contracted-CFT Correspondence. *JHEP*, 06:134, 2014.

[232] Ahmed Almheiri, Xi Dong, and Daniel Harlow. Bulk Locality and Quantum Error Correction in AdS/CFT. *JHEP*, 04:163, 2015.

[233] Marco Astorino. CFT Duals for Accelerating Black Holes. *Phys. Lett. B*, 760:393–405, 2016.

[234] Michael Appels, Ruth Gregory, and David Kubiznak. Thermodynamics of Accelerating Black Holes. *Phys. Rev. Lett.*, 117(13):131303, 2016.

[235] Maulik Parikh and Prasant Samantray. Rindler-ads/cft. *Journal of High Energy Physics*, 2018(10):129, 2018.

[236] Andrés Anabalón, Finnian Gray, Ruth Gregory, David Kubizňák, and Robert B. Mann. Thermodynamics of Charged,

Rotating, and Accelerating Black Holes. *JHEP*, 04:096, 2019.

[237] Andrés Anabalón, Michael Appels, Ruth Gregory, David Kubiznák, Robert B. Mann, and Alī Ovgün. Holographic Thermodynamics of Accelerating Black Holes. *Phys. Rev. D*, 98(10):104038, 2018.

[238] Ruth Gregory and Andrew Scoins. Accelerating Black Hole Chemistry. *Phys. Lett. B*, 796:191–195, 2019.

[239] Pietro Ferrero, Jerome P. Gauntlett, Juan Manuel Pérez Ipiña, Dario Martelli, and James Sparks. Accelerating black holes and spinning spindles. *Phys. Rev. D*, 104(4):046007, 2021.

[240] Davide Cassani, Jerome P. Gauntlett, Dario Martelli, and James Sparks. Thermodynamics of accelerating and supersymmetric AdS4 black holes. *Phys. Rev. D*, 104(8):086005, 2021.

[241] Sotaro Sugishita and Seiji Terashima. Rindler bulk reconstruction and subregion duality in AdS/CFT. *JHEP*, 11:041, 2022.

[242] Jose Barrientos, Adolfo Cisterna, David Kubiznak, and Julio Oliva. Accelerated black holes beyond Maxwell’s electrodynamics. *Phys. Lett. B*, 834:137447, 2022.

[243] Di Wu. Topological classes of thermodynamics of the four-dimensional static accelerating black holes. *Phys. Rev. D*, 108(8):084041, 2023.

[244] Xin-Xiang Ju, Wen-Bin Pan, Ya-Wen Sun, and Yuan-Tai Wang. Generalized Rindler Wedge and Holographic Observer Concordance. 2 2023.

[245] Gabriel Arenas-Henriquez, Adolfo Cisterna, Felipe Diaz, and Ruth Gregory. Accelerating Black Holes in 2+1 dimensions: Holography revisited. *JHEP*, 09:122, 2023.

[246] Xin-Xiang Ju, Bo-Hao Liu, Wen-Bin Pan, Ya-Wen Sun, and Yuan-Tai Wang. Squashed entanglement from generalized Rindler wedge. *JHEP*, 09:006, 2025.

[247] Harald Dorn and Thanh Hai Ngo. On the internal space dependence of the static quark-antiquark potential in $N = 4$ SYM plasma wind. *Phys. Lett. B*, 654:41–45, 2007.

[248] Nadav Drukker and Valentina Forini. Generalized quark-antiquark potential at weak and strong coupling. *JHEP*, 06:131, 2011.